EVALUATION OF GENE EXPRESSION DURING DEVELOPMENT OF THE NEONATAL PORCINE UTERUS USING SUPPRESSION SUBTRACTIVE HYBRIDIZATION

by

LEANNE MICHELLE WIER

Bachelor of Science

Texas A&M University

College Station, Texas

2000

Submitted to the Faculty
of the Graduate College of
Oklahoma State University in
partial fulfillment for the degree of
MASTER of SCIENCE
December 2004

EVALUATION OF GENE EXPRESSION DURING

DEVELOPMENT OF THE NEONATAL

PORCINE UTERUS USING

SUPPRESSION SUBTRACTIVE

HYBRIDIZATION

Thesis Approved:

Rodney D. Geisert
Thesis Advisor

Jerry R. Malayer

Clint R. Krehbiel

A. Gordon Emslie
Dean of the Graduate College

Acknowledgements

I would like to thank my advisors for serving on my committee and providing the opportunity to earn a Master of Science degree. Thank you Dr. Rod Geisert for allowing me to work on this project under your instruction. I am grateful for your commitment and inspiration for quality work in the field of reproductive physiology. Thank you Dr. Clint Krehbiel for serving on my committee and providing sound academic guidance throughout my time at OSU. Special thanks is due to Dr. Jerry Malayer who has been a great advisor, mentor, and employer. I appreciate you having hope in my abilities from the beginning and allowing me to work in your laboratory.

To Amy Hurst, thank you for all of your help in and outside of the laboratory. Your guidance and friendship has proven invaluable and will never be forgotten. To Jason Ross and Morgan Ashworth: thank you for your support and help with everything from tissue collection to laboratory techniques. I could not have gotten this project completed without the two of you. To all of the people working with me in the laboratory over the years: Mahesh Mohan, Lisa Whitworth, Lori Green Vandeventer, Mason Reichart, Misti Spatz, T.R. Nagaraja, Dave Goad, and Akhilesh Ramachandran, thank you for your wisdom and encouragement. Finally, I would like to give acknowledgement to Dan May for his unconditional support. I would not have pursued this degree if it were not for your encouragement. Thank you.

Table of Contents

List of Tables

List of Figures

Abbreviations

Acronym	Name
αFP ……	Alpha fetoprotein
β-NAD……..	Beta- Nicotinamide adenine dinucleotide
BSA……	Bovine Serum Albumin
Ca^{++}……...	Calcium
$\Delta\Delta C_T$……..	Calibrated Value
cDNA…….	Complementary Deoxyribonucleic Acid
CL……..	Corpus Luteum
COL1A2……	Procollagen, type I, alpha 2
COL3A1……	Procollagen, type III, alpha 2
DEPC…….	Diethyl pyrocarbonate
DIG……	Digoxigenin
DNA……..…	Deoxyribonucleic Acid
dNTP……	Deoxy Nucleotide Triphosphate
DTT……..…	Dithiothreitol
E. coli……	Escherichia coli
EB……..	Estradiol benzoate
EDTA……	Ethylenediaminetetraacetic Acid
EF1a1……	Elongation Factor 1 alpha 1

Acronym	Name
ER……..	Estrogen Receptor
ERKO……	Estrogen Receptor Knockout
EtBr……	Ethidium Bromide
EV……..	Estradiol-17β valerate
FGF-10……..…	Fibroblast growth factor 10
FGF-7……	Fibroblast growth factor 7
$2^{-\Delta\Delta CT}$……...	Fold Difference
G3PDH……..…	Glyceraldehyde-3-Phosphate Dehydrogenase
HEPES……	4-2-Hydroxyethyl-1-Piperazineethanesulfonic Acid
HGF……	Hepatocyte growth factor
ICI……..	ICI 182,780
IGF-I……..	Insulin like growth factor I
IGF-II…….	Insulin like growth factor II
IGF-IIR……..	Type II insulin like growth factor receptor
IGF-IR……	Type I insulin like growth factor receptor
IPTG……..	Isopropyl b-D-thiogalactopyranoside
KOAc…….	Potassium Acetate
µl……	Microliter
µM……..	Micromole
mg……..…	Milligram
mM……	Millimole
MW……	Molecular Weight
ΔC_T……	Normalized Cycle Threshold

Acronym	Name
OVX……	Ovariectomy
PABPC1……..	Poly(A) Binding Protein, Cytoplasmic 1
PCR ……..	Polymerase Chain Reaction
PI……	Plasmin/trypsin inhibitor
PND……..	Post Natal Day
POLR2C……	Polymerase II Polypeptide C
qRT-PCR……	Quantitative Real-Time PCR
RABP……..….	Retinoic Acid Binding Protein
RAR……	Retinoic acid receptor
RBP……	Retinol binding protein
RNA……	Ribonucleic Acid
RPM……	Rotations Per Min
RT……..	Reverse Transcription
rt……	Room temperature
SPARCL1……..	Secreted protein, acidic, rich in cysteine-like 1
SSH……	Suppression Subtractive Hybridization
TAE……	Tris-acetate-EDTA buffer
TGF-β ……	Transforming growth factor-β
V……	Volts
X-GAL……	5-Bromo-4-chloro-3-indolyl- β-D-galactopyranoside
ZP……	Zona Pellucida

Chapter 1: INTRODUCTION

Uterine gland morphogenesis and growth is a postnatal event in pigs [Hadek and Getty, 1959; Bal and Getty, 1970; Spencer *et al.*, 1993a], sheep [Wiley *et al.*, 1986; Bartol *et al.*, 1988a; 1988b], and rodents [Branham *et al.*, 1985]. The impact that uterine glands have throughout pregnancy is mediated through synthesis and secretion of a complex assortment of proteins collectively known as histotroph [Roberts and Bazer, 1988]. Porcine uterine histotroph aids in regulation of conceptus survival and development [Bazer, 1975], initiation of steroidogenesis for production of estrogen needed for maternal recognition of pregnancy, early placentation, and conceptus survival [Bazer, 1975; Roberts and Bazer, 1988]. Composition of histotroph in various farm species is dependent upon stage of estrous cycle or pregnancy [Roberts and Bazer, 1988] and includes growth factors, hormones, transport proteins, and other progesterone-induced proteins [Trout *et al.*, 1992; Spencer *et al.*, 1999].

Uterine secretions are critical for conceptus survival, particularly in species where there is an extended period prior to trophoblast attachment and placentation. The impact that histotroph has on conceptus survival is apparent from studies in ewes in which uterine gland development can be inhibited perinatally by endocrine disruption, which alters subsequent adult uterine structure [Gray *et al.*, 2001c] and function [Bartol *et al.*, 1993; Tarleton *et al.*, 2003].

The porcine uterus is not completely differentiated at birth; with

differentiation being initiated prenatally and completed postnatally [Hadek and Getty, 1959; Bal and Getty, 1970; Spencer *et al.*, 1993a; Tarleton *et al.*, 2001]. Uterine gland morphogenesis (adenogenesis) begins at birth and rapidly develops to functional maturity by 120 days. The histological morphology of the porcine neonatal uterus begins with the differentiation of glandular epithelium (GE) from the luminal epithelium (LE), which is followed by proliferation, tubular coiling, and branching of the GE deep into the uterine stroma [Spencer *et al*., 1993a].

The mechanisms involved with uterine adenogenesis are regulated locally, independent of the ovary [Wu and Dziuk, 1988; Spencer *et al.*, 1993a]. Uterine adenogenesis occurs through changes in cell proliferation and movement, cell-to-cell interaction, alterations in extracellular matrix (ECM), and many paracrine pathways [Bartol *et al.*, 1993; Gray *et al.*, 2001b]. Epithelial differentiation is regulated by stromal growth factors (and their respective receptors) such as fibroblast growth factor (FGF)-7, FGF-10, hepatocyte growth factor (HGF), transforming growth factor-β (TGF-β), and insulin like growth factor (IGF)-I and II are key for gland differentiation and proliferation [Taylor *et al.*, 2001; Gray *et al.*, 2001b].

The regulation of adult porcine uterine gland function is dependent upon conceptus secretion of estrogen in early pregnancy to signal maternal recognition of pregnancy [Geisert *et al.*, 1982c]. Conceptus secretion of estrogens induce sequestering of $PGF_{2\alpha}$ in the uterine lumen to prevent luteolysis. As a result, corpora lutea (CL) are maintained and continue to secrete progesterone needed for maintenance of pregnancy to term [Bazer *et al.*, 1984; Geisert *et al.*, 1994]. Increasing plasma content of progesterone stimulates uterine protein secretions which increase during the luteal phase of the estrous cycle and early pregnancy. Several progesterone-induced proteins such as uteroferrin [Bazer and Roberts, 1983; Bazer *et al.*, 1984], retinol binding

protein (RBP) [Clawitter *et al.*, 1990], lysozyme [Roberts *et al.*, 1993], plasmin/trypsin inhibitor (PI) [Roberts *et al.*, 1993], and IGF-I [Simmen and Simmen, 1990] have been isolated in the uterus during pregnancy and are considered to be important factors for conceptus survival.

Specific changes in gene expression involved in the completion of uterine gland development during the first 56 days of postnatal growth in the pig have not been well described or understood. Therefore, the objective of this study was to identify differentially expressed genes involved in uterine gland development in the neonatal pig uterus using suppression subtractive hybridization (SSH). Characterization of the gene expression profile for early postnatal uterine development in the pig will help determine biological significance and aid in strategies for improved reproductive potential.

Chapter 2: LITERATURE REVIEW

2.1 Uterine Gland Morphogenesis in Rodents and Domestic Farm Animals

Morphogenesis of tissues occurs as groups of cells undergo organized changes in cellular events which lead to a change in the tissue form and function [Bernfield, 1981]. Uterine morphogenesis begins during embryonic development of the paramesonephric or Müllerian ducts [Marion and Gier, 1971]. Initial uterine morphogenesis begins with the organization of the two functional compartments of the uterus, the endometrium and myometrium [Bartol *et al.*, 1993]. Histogenesis of the endometrium involves stratification of undifferentiated mesenchyme into either a dense stromal zone (stratum compactum) characteristic of the luminal epithelium (LE) or loosely organized stromal zone (stratum spongiosum) for which the characteristic glandular epithelium (GE) will differentiate and invade. Myometrial differentiation is also initiated forming the inner circular and the outer longitudinal smooth muscle layers of the mature uterus [Bartol *et al.*, 1993; Gray *et al.*, 2001b]. After development of the inner mucosal endometrium and inner and outer smooth muscle myometrium, there is a coordinated development of the histoarchitecture of the uterus [Bartol *et al.*, 1993], which is species specific, as illustrated in Figure 2.1.

Uterine morphogenesis in sheep, cattle, mice, and pigs occurs in a progressive manner, initiated prenatally and completed postnatally, at some point before puberty.

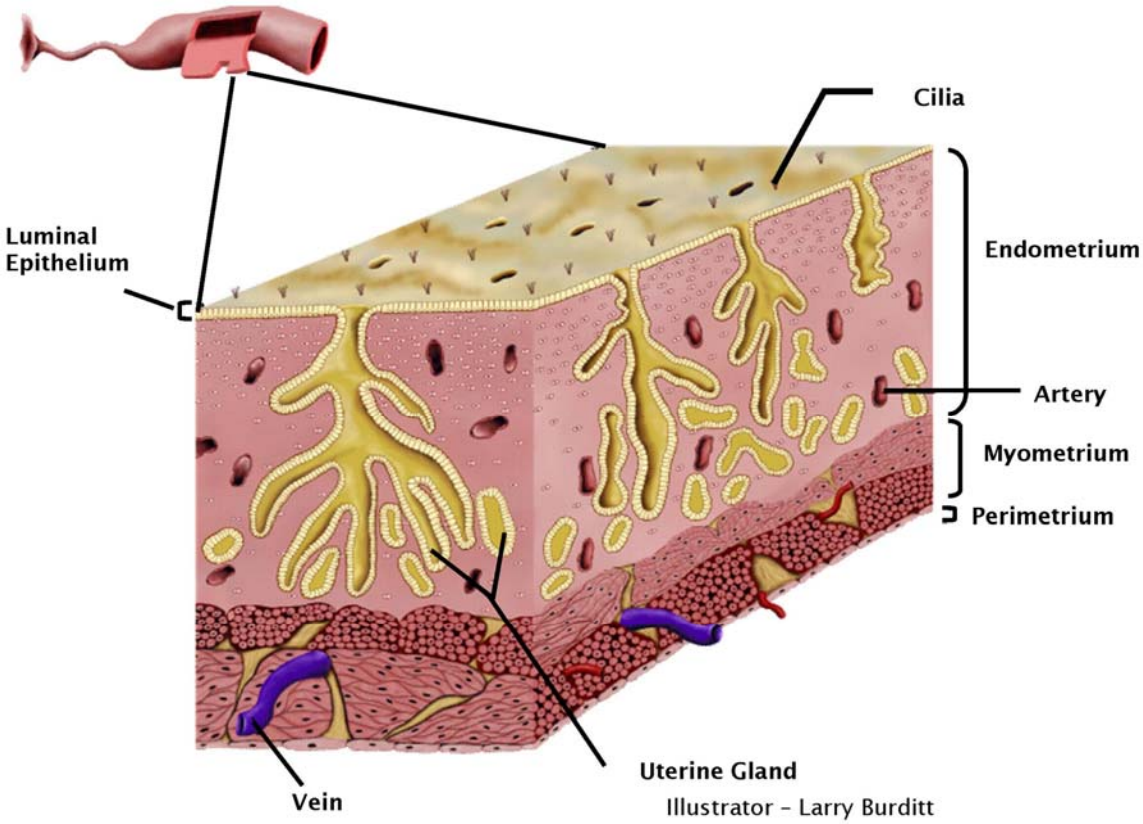

Figure 2.1. Histoarchitecture of the porcine uterus. The mature pig uterus is composed of two functional compartments, the endometrium and myometrium and each compartment is subdivided. The innermost layer at the lumen is the luminal epithelium that lines the uterus. The glandular epithelium penetrates deep into the endometrium and functions to secrete proteins into the uterine lumen in early pregnancy. The myometrium is composed of the inner circular and outer longitudinal layers.

While the type of placentation and length of gestation differ between species, the pattern of uterine differentiation was similar [Wiley *et al.*, 1986]. Although similar, postnatal uterine gland development in livestock species includes uterine gland coiling and branching, whereas there is no tight coiling or branching of the uterine glands in rodents [Mossman, 1987].

Sheep and Cattle

A morphological difference in the endometrium of ruminants compared to other species is the presence of multiple aglandular caruncules. Caruncles are LE-covered

dense stroma sites for synepitheliochorial placentation and nutrient exchange whereas the intercaruncular areas have abundant uterine glands [King *et al.*, 1980; 1981].

Uterine morphogenesis in ruminants, such as cattle and sheep, begins when the embryonic paramesonephric duct fuses leading to the formation of a bicornuate uterus, and is attained between Days 34 and 55 of gestation in sheep [Wiley *et al.*, 1986],. Distinct raised luminal clefts are apparent which later develop into caruncles by Day 90 of gestation in sheep [Wiley *et al.*, 1986]. The stratum compactum and stratum spongiosum are visible, and the inner circular and outer circular layers appear to be differentiating at this time. Between gestational Days 135 and 150 in sheep [Wiley *et al.*, 1986] and at Day 250 in cattle [Marion and Gier, 1971; Atkinson *et al.*, 1984], uterine gland morphogenesis is initiated, as seen by the presence of shallow depressions in the LE. In the ewe, adenogenesis is initiated at the time of birth when progesterone is removed from the fetal environment [Gray *et al.*, 2000b].

At postnatal day (PND) 0, or birth, shallow epithelial depressions are visible in sheep at the presumptive intercaruncular (glandular) sites. Epithelial buds proliferate and begin to invade through the uterine stroma between PND 7 and 14. Wiley and coworkers [1986] noted the presence of tubular glands at PND 9. By PND 21, these tubes begin to coil and branch, continuing branching morphogenesis after PND 21 so that glands extend to the myometrium by PND 26 [Wiley *et al.*, 1986; Gray *et al.*, 2001b]. Although the uterine endometrium is histoarchitecturally similar to the adult by PND 56, complete uterine maturation may not be accomplished until puberty or establishment of pregnancy [Kennedy *et al.*, 1974].

In sheep, endometrial gland differentiation can be inhibited by neonatal exposure to progestins, creating a uterine gland knockout (UGKO) phenotype [Bartol *et al.*, 1988b]. Disruption of normal glandular developmental patterns with exogenous progestin is specific to adenogenesis, as development of the myometrium and other

uterine structures are not affected [Gray *et al.*, 2000b; 2001a; 2002]. Uterine glands of UGKO ewes do not penetrate the intercaruncular stroma, neither is there an identifiable stratum compactum, as in the normal phenotype [Gray *et al.*, 2001a]. Therefore, UGKO ewes offer an insight to the mechanisms involved in neonatal adenogenesis. Gray and coworkers [2000a] administered norgestomet (a synthetic progestin) for 8, 16, or 32 weeks to neonatal ewes and found that exposure for as short as 8 weeks was sufficient to inhibit uterine gland development.

Fertility is negatively affected in UGKO ewes, as there is a failure to establish pregnancy due to conceptus death during the peri-implantation period [Gray *et al.*, 2002]. Endocrine disruption of early postnatal gland development influences uterine secretions by altering the morphological glandular composition of the uterine intercaruncular area. As a result of the lack of uterine glandular development in the neonatal uterus, histotroph is not adequately synthesized or secreted. Gray and coworkers [2001c] demonstrated the presence of healthy conceptuses in UGKO ewes on Days 6 and 9 of pregnancy, but no conceptuses or only tubular, nonelongated conceptuses were present on Day 14.

Uterine protein secretions that are involved in mediating the ovine maternal-conceptus interaction are altered in the UGKO phenotype. Many of the uterine secreted factors are critical to conceptus survival during implantation, including mucin 1 (Muc-1), glycosylation-dependent cell adhesion molecule 1 (GlyCAM-1), and osteopontin (OPN). Mucin 1 (Muc-1) inhibits cell-cell and cell-ECM interactions [Komatsu *et al.*, 1997] and is presumably involved in regulation of conceptus trophectoderm adhesion to maternal LE [DeSouza *et al.*, 2000]. Johnson and coworkers [2001] showed Muc-1 to be localized to the apical surface of the LE and GE. Glandular epithelium muc-1 expression was high throughout the estrous cycle and early pregnancy, while LE expression decreased. Expression of Muc-1 in UGKO ewes was not different from normal ewes [Gray *et al.*,

2002]. The role that the secreted protein osteopontin serves during early pregnancy may be as an adhesion molecule during conceptus attachment [Johnson *et al.*, 1999a; 1999b]. In pregnancy, OPN has been shown to be restricted to the endometrial glands of Day 13 to 19 pregnant ewes [Johnson *et al.*, 1999a]. Immunological detection of OPN showed the protein to be present on the luminal and glandular epithelial cells of the uterus [Johnson *et al.*, 1999b], but was undetectable in UGKO ewes [Gray *et al.*, 2002]. Interferon τ (IFNτ) is the ovine maternal recognition of pregnancy signal [Bazer *et al.*, 1997] that is secreted during conceptus elongation. This critical developmental factor was shown to be absent in flushings from UGKO ewes whether conceptus was absent, degenerated tubular conceptus, or fragmented filamentous conceptus [Gray *et al.*, 2002]. In the absence of uterine glands, conceptus development is defective and pregnancy cannot be maintained. These results indicate secretions from the uterine glands are essential for conceptus development and attachment to the uterine surface.

Rodents

On gestational Day 15-16, the embryonic paramesonephric duct partially fuses in rats and mice to form a bicornuate uterus [Mossmann, 1987]. At birth, about 4 days after paramesonephric duct fusion, the uterus of female mice and rats are still devoid of endometrial glands. The endometrium consists of a simple epithelium maintained on an undifferentiated mesenchyme. The GE begins to bud by PND 5, creating epithelial invaginations. Simple, tubular glands are not apparent until PND 7 in mice and PND 9 in rats. In rats, these events correlate with elevated serum estradiol levels and increased uterine sensitivity to estradiol [Branham *et al.*, 1985].

Rodent endometrial gland differentiation is inhibited by exposure with the antiestrogen tamoxifen [Branham *et al.*, 1985]. Responses to tamoxifen are dependent upon the dose and period of exposure, resulting in either an agonist or antagonist

response. For example, neonatal rats treated with tamoxifen initiated early myometrial differentiation, but delayed the emergence of endometrial glands [Branham *et al.*, 1985].

2.2 Developmental Biology of Porcine Uterine Gland Morphogenesis

During porcine conceptus development, the paramesonephric ducts fuse at the caudal ends, resulting in the formation of a short uterine body and extensive uterine horns [Mossman, 1989]. Postnatal development of pig uterine glands begins at birth and rapidly reaches functional maturity by PND 120 [Hadek and Getty, 1959]. Morphogenesis of functional uterine glands is necessary for normal uterine function and conceptus survival. The histological conformation of the porcine uterus during early postnatal development has been characterized in detail including the anatomical changes throughout the differentiation and budding of GE from the LE followed by proliferation, tubular coiling, and branching into the uterine stroma [Hadek and Getty, 1959; Bal and Getty, 1970; Bartol *et al.*, 1993; Spencer *et al.*, 1993a; Tarleton *et al.*, 1998].

Postnatal uterine gland development has been shown to be related to age of the animal [Hadek and Getty, 1959]. At the time of birth, or PND 0, the uterine wall is undifferentiated [Bal and Getty, 1970] with only shallow epithelial depressions [Hadek and Getty, 1959] (Figure 2.2 A), which are believed to be the predecessor for the uterine glands of the adult pig uterus [Hadek and Getty, 1959; Bartol *et al.*, 1993]. There is no distinct outer longitudinal layer of myometrium, but an inner circular layer is present [Bal and Getty, 1970]. At this time, the thickness of the uterine wall is increasing and the weight of the endometrium is about 55% of the total uterine wall thickness [Hadek and Getty, 1959].

By PND 7, the uterine glands appear as coiled tubular glands in the shallow stratum compactum while the stratum spongiosum is becoming thicker and many tubular glands can be observed by PND 14 (Figure 2.2 B) [Spencer *et al.*, 1993a; 1993b]. The glands are described as having “large, funnel-like openings” [Hadek and Getty, 1959] and coil throughout the top one-third of the endometrium [Spencer *et al.*, 1993a].

Distinct tubular glands have begun to branch throughout the endometrium by PND 28 and GE can be observed within the uterine stroma (Figure 2.2 C). Furthermore, uterine mucosal folds begin to develop and increase the uterine surface area [Hadek and Getty, 1959; Bal and Getty, 1970].

By PND 56, uterine glands are dense and extensive. At this time, the glands are coiled, branched, and extend from the luminal surface to the myometrium (Figure 2.2 E). In addition, the endometrial folds and the inner circular and outer longitudinal myometrium are well-developed [Spencer *et al.*, 1993a; Bartol *et al.*, 1993]. Growth of the uterus and its functional compartments continue to grow in a prolific manner while the endometrial folds continue to grow in a more unpredictable manner [Hadek and Getty, 1959] until the uterus reaches functional maturity by PND 120 [Hadek and Getty, 1959; Bal and Getty, 1970].

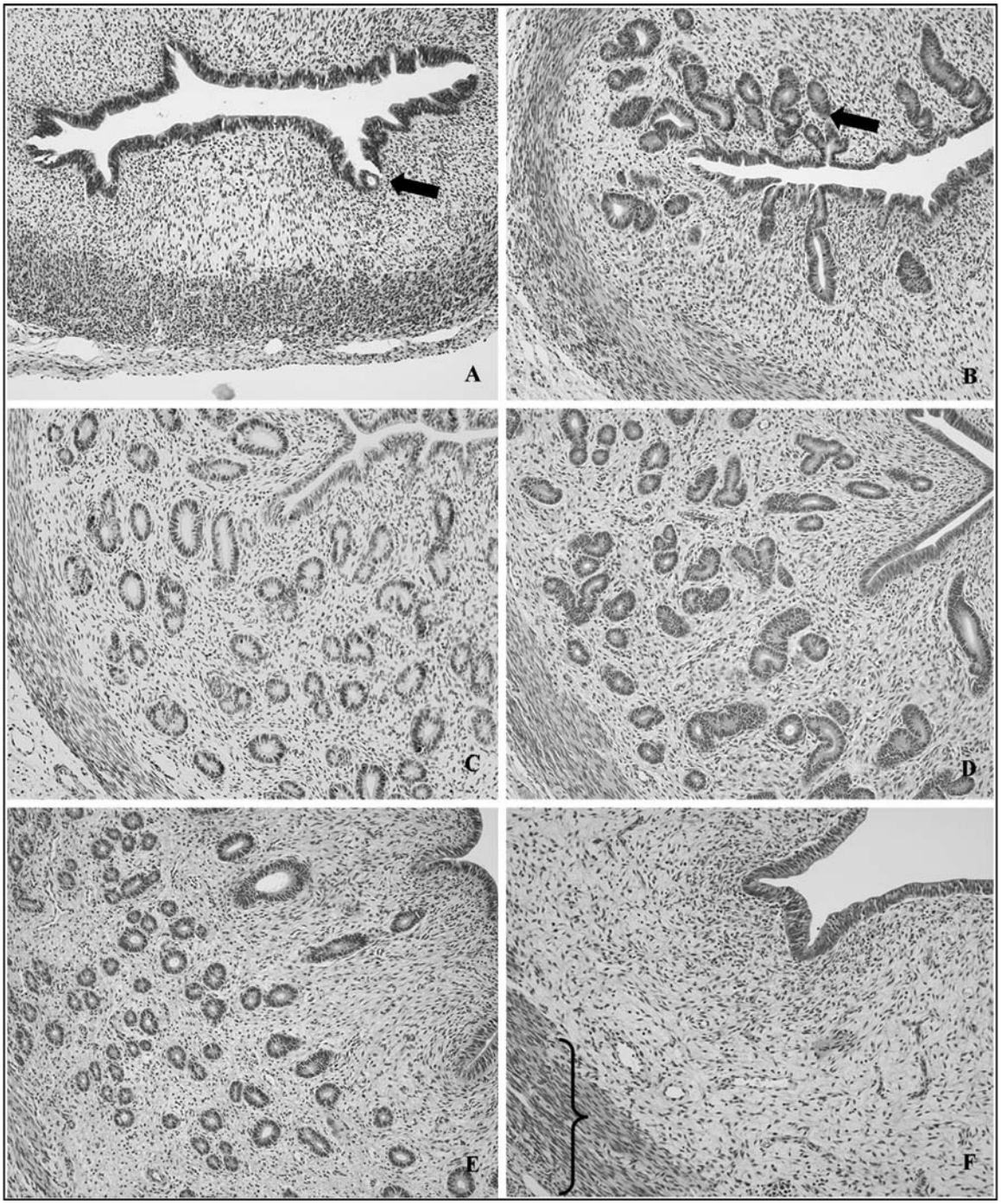

Figure 2.2. Histological view of the changing morphology of the developing neonate pig uterus. Panel A) PND 0: Shallow epithelial depressions (black arrow) can be observed. B) PND 14: Tubular glands begin to coil and branch (black arrow). C) PND 28: Continued glandular branching morphogenesis. D) PND 42: Branching morphogenesis continues. E) PND 56: Glands are now dense and extensive throughout the endometrium. F) PND 42 with abnormal uterine gland development.

Note the absence of glands, thick endometrium, and thick myometrium (brace). All images were taken at 10 x.

2.3 Regulation of Porcine Uterine Gland Morphogenesis

Tissue morphogenesis is a result of the synchronization of cellular activities that include cell adhesion, proliferation, apoptosis, and changes in cell shape, ultimately initiating cell movement [Bernfield, 1981]. Based on the regulatory pathways for gland development in other epitheliomesenchymal organs, porcine uterine gland morphogenesis is likely to be regulated locally [Spencer *et al.*, 1993a] by several factors including changes in:

- Cell proliferation and movement
- Paracrine cell-to-cell and cell-to-extracellular matrix interactions [Bartol *et al.*, 1993; Gray *et al.*, 2001b]
- Secretion of many biochemical factors [for review see Gray *et al.*, 2001b]

Changes in cell proliferation and movement

Spencer and coworkers [1993a] indicated that the increased synthesis of DNA in epithelial cells, with steady decrease in the stromal cells, is indicative of the emergence of uterine glands via budding of the GE from LE in the neonate pig, rather than a result of cell proliferation. Furthermore, histochemical studies at the stromal-epithelial boundary provide evidence that bud outgrowth and invagination does not require localized cell proliferation [Spencer *et al.*, 1993a].

Epithelial DNA synthesis during uterine adenogenesis is regulated sequentially and locally in a tissue microenvironment [Bartol *et al.*, 1988b; Spencer *et al.*, 1993a; Gray *et al.*, 2001b], likely a result of epithelial-mesenchymal interactions. The conditions of this local microenvironment are vital for the proliferation of glands [Bartol *et al.*, 1988a]

which is possibly an effect of the stroma to allow a localized response to hormones [Cunha and Lung, 1979].

Changes in cell-to-cell interactions

Sharpe and Ferguson [1988] stated that epithelial-mesenchymal interactions lead to an alteration of either or both tissues that would not have taken place had the interaction not occurred. This type of interaction is known to support and regulate the morphogenesis of many organs [Bernfield, 1981], including the uterus [Gray *et al.*, 2001b] by locally controlling cell movement, adhesion, differentiation, and proliferation [Sharpe and Ferguson, 1988; Taylor *et al.*, 2001; Gray *et al.*, 2001b].

Cunha and Lung [1979] demonstrated in the mouse that uterine stroma directs morphogenesis of the uterine epithelium as bladder epithelium could be transformed to uterine epithelium if placed over uterine stroma. Additional rodent tissue recombination studies suggest in the developing neonate uterus that the mesenchyme dictates the epithelial developmental pattern while presence of the epithelium allows for the organization of uterine stroma and differentiation of myometrium [Cunha, 1976; Cunha *et al.*, 1983].

Developmental epithelial-mesenchymal interactions tend to be reciprocal in relation to time. For the most part, the epithelium will signal to the mesenchyme, which subsequently signals back to the epithelium. This signaling occurs in such a way to allow for organized regulation of cell proliferation, differentiation, and morphogenesis [Sharpe and Ferguson, 1988].

When the epithelial-mesenchymal interaction is disrupted, normal morphogenesis is unable to take place. For example, UGKO ewes treated with a progestin implant for 32 weeks after birth lack the ability to develop uterine glands [Gray *et al*., 2000a]. The UGKO ewes exhibit a simple LE over a dense stroma, but appeared

to have normal myometrial development. It is likely that this prepubertal exposure to progestin interrupts the normal epithelial-mesenchymal interaction to prevent proper development of the uterus [Spencer *et al.*, 1999; Taylor *et al.*, 2001].

Changes in cell-to-extracellular matrix interactions

The ECM functions as a supportive framework that serves to facilitate individual cells to function as a unit. It is comprised of fibrous proteins, glycosaminoglycans (GAG's), glycoproteins, and interstitial fluid [Bernfield, 1981]. Included in the GAGs are hyalauronic acid (HA), sulfated GAGs (SGAGs), chondroitin sulfate (CS), heparan sulfate (HS), and keratan sulfate [Bartol *et al.*, 1993].

Interactions of the ECM during uterine adenogenesis, as in other tissue morphogenesis, involve the presence of collagens for structural organization, GAG concentration to dictate matrix association (loose, soft, firm, or rigid), and glycoproteins such as fibronectin to serve as adhesion proteins. This close association of cells via the ECM allows for normal cellular activities [for review, see Bernfield, 1981].

Bernfield [1981] showed in the developing mouse embryo salivary gland that epithelial-mesenchymal interaction through the organization and remodeling of ECM not only influences morphogenesis, but is reliant on this interaction. Also critical during this process is the presence of a basal lamina for epithelium to anchor to which its structural integrity is dependent on GAG.

The turnover rate of basal lamina GAG is different for various sites of developing tissues [Bernfield, 1981]. Sites with a lower GAG turnover rate are indicative of quiescence, while areas with a higher GAG turnover rate suggest morphogenetic sites in which disruptions in the lamina are present. Degradation of mesenchymal non-sulfated GAG is most apparent at the distant lobules during branching morphogenesis where

cells proliferate rapidly, whereas there is less cell proliferation at the glandular clefts and lower sulfated GAG turnover rates.

Spencer and others [1993a] localized GAG distribution during uterine morphogenesis in the neonate pig through antibody staining. These authors found that at PND 0, GAG staining was uniform throughout the uterus. By PND 7, the GAG distribution was well defined in the shallow stroma beneath the LE, in clefts at the LE and GE junctions, and in stroma bordering the developing necks of glands. This pattern persisted through PND 28, but staining intensity was weakened by PND 56. These data are consistent with the theory that areas that are morphogenetically inactive and stable will exhibit the more intense GAG staining, whereas the areas with high GAG turnover rates and morphogenetic activity exhibit lesser staining.

The distribution of ECM collagen during regulation of glandular morphogenesis is critical for structural integrity of the tissue by reducing basal lamina GAG degradation [Spencer *et al.*, 1993a]. Furthermore, the ECM can control the cell cycle, apoptosis, and epithelial gene expression to ultimately influence branching morphogenesis [Gray *et al.*, 2001b].

Changes in interactions between biochemical communication pathways

Cell communication between the epithelium and mesenchyme in the uterus is both paracrine and autocrine [Cooke *et* al., 1998; Taylor *et al.*, 2001; Gray *et al.*, 2001b]. Epithelial cell proliferation, differentiation, branching morphogenesis, cell migration, ECM synthesis and degradation, and angiogenesis are all effected by growth factors and their receptors [Sharpe and Ferguson, 1988; Gray *et al.*, 2001b].

Stromal Growth Factors

Stromal-derived growth factors are essential for gland proliferation, differentiation, branching morphogenesis, and tissue remodeling in epithelial-

mesenchymal organogenesis [Taylor *et al*., 2001]. Stromal paracrine factors involved with gland morphogenesis include fibroblast growth factor (FGF)-7 [Igarashi *et al*., 1998], FGF-10 [Yamasaki *et al*., 1996; Beer *et al*., 1997; Bellusci *et al*., 1997], hepatocyte growth factor (HGF), transforming growth factor-β (TGF-β) and insulin like growth factor (IGF)-I and II [for review, see Taylor *et al.*, 2001].

The fibroblast growth factors are paracrine growth factors that accelerate epithelial cell proliferation and differentiation by interacting with their cell surface receptors (FGFR) that initiate tyrosine kinase activity [for review, see Powers *et al*., 2000]. Cell surface heparan sulfate proteoglycan (HSPG) serves as a co-receptor for complete FGFR activation [Dillon *et al.*, 2004].

Expression of FGF-7 is localized primarily to the stromal component (tunica muscularis) of blood vessels in endometrium and myometrium of the adult ewe [Chen *et al*., 2000] but not detectible in neonatal uteri, despite continuous mRNA expression from PND 1 to 56 [Taylor *et al.*, 2001]. In the neonatal ovine uterus, the receptors are expressed only in the LE on PND 1, then expression becomes abundant in the GE between PND 7 and 56 [Taylor *et al.*, 2001]. Data of FGF-7 ligand and receptor transcription in mouse tissue suggests that FGF-7 acts in a paracrine manner on epithelial cells [Beer *et al.*, 1997], since the ligand is primarily produced by fibroblasts and endothelial cells, but not epithelial cells, while the receptor is expressed on epithelial cells. The role of FGF-7 during neonate uterine adenogenesis is likely for initiating epithelial cell proliferation [Taylor *et al.*, 2001].

Fibroblast growth factor-10 was initially isolated from embryonic rat tissues [Yamasaki *et al.*, 1996] and proposed to be associated with patterning early branching morphogenesis of the lung [Bellusci *et al.*, 1997]. Fibroblast growth factor-10 is primarily cell- or ECM-associated [Igarashi *et al.*, 273], mitogenic for epithelial cells, and binds to both FGFR1IIIb and FGFR2IIIb [Powers *et al*., 2000]. In the rat lung, FGF-10 is a short-

range signal and puts forth only a modest effect during lung epithelial bud development [Park *et al.*, 1998]. This is evident when FGF-10 alone was not adequate to completely promote lung bud migration, but was completed upon the addition of FGF-7 [Park *et al.*, 1998]. Based on the function of FGF-10 in the lung, a hypothesis regarding neonate uterine adenogenesis can be developed. In the cyclic and pregnant ovine uterus, FGF-10 is expressed in the endometrial stroma, while its receptor is localized only to the epithelium [Chen *et al.*, 2000]. Gene expression of FGF-10 in the neonatal ovine uterus did not change from PND 1 to 21 but increased after PND 21 [Taylor *et al.*, 2001], the time when branching morphogenesis occurs [Wiley, *et al*., 1986]. Taylor and coworkers [2001] suggested that FGF-10 serves as a chemotactic molecule to stimulate gland budding in neonate uteri.

Hepatocyte growth factor serves as a paracrine factor to mediate paracrine epithelial-mesenchymal interactions during morphogenesis of the lung [Rubin *et al.*, 1991] and mammary gland [for review, see Pollard, 2001]. The *c-met* proto-oncogene product mediates the mitogenic, motogenic, and morphogenic actions of HGF [Bottaro *et al.*, 1991]. Gene expression of HGF increased after PND 21 similar to FGF-10 during ovine uterine gland branching morphogenesis, implying a synergistic effect between FGF-10 and HGF [Taylor *et al.*, 2001]. Tissue expression of HGF receptor *c-met* is localized to the LE and upper GE in the stratum compactum of the neonatal ovine uterus.

Transforming growth factor-β is a cytokine with many functions and activities that include cell-cycle control, regulation of early development, differentiation, extracellular matrix formation, immune functions, and the induction of apoptosis [for review see Norbert and Krieglstein, 2002]. It binds to its membrane-bound receptors, TGF-β receptor I and II. Synergistic effects of TGF-β with other growth factors is one possible explanation for its multifunctional properties. During development of the mouse

mammary gland, TGF-β is necessary for regulation of side branching during branching morphogenesis. It has been shown to be down-regulated at sites where side branches have begun to form. When TGF-β receptor signaling is inhibited in the mouse mammary gland, excessive duct branching occurs [Wiseman and Werb, 2002].

Insulin-like Growth Factors

Insulin-like growth factor I and II are structurally similar to proinsulin and possess insulin-like effects [Wang and Chard, 1999]. Both IGF-I and II are synthesized *de novo* in multiple tissues and exhibit mitogenic effects in the tissue via autocrine and/or paracrine mechanisms. Furthermore, the IGF system can mediate tissue response to steroids, such as the effects of estrogen on the growth and development of the rodent uterus [Murphy and Ghahary, 1990].

Insulin-like growth factor I is primarily produced by the liver and its secretion is mediated by growth hormone (GH) action through its receptor (GHR) [Wiseman and Werb, 2002]. Type I (IGF-IR) and type II (IGF-IIR) IGF cell membrane receptors mediate the biological effects of IGF-I and II. Type I receptors have a high affinity for IGF-I binding, but also bind IGF-II and insulin at higher concentrations. Type II receptors bind only IGFs, and have a higher affinity for IGF-II [Wang and Chard, 1999].

Research has indicated the necessity of IGF-I for normal development of the reproductive system of both sexes [Baker *et al.*, 1996]. The absence of IGF-I in female mice inhibits myometrial maturation and development of graafian follicles on the ovaries [Cerro and Pintar, 1997]. Follicular content of IGF-I increases in the pig after treatment with gonadotropins or GH, whereas IGF-II concentrations remain unchanged [Hammond *et al.*, 1993]. Expression of IGF-I and –II is localized to the stroma of the adult ovine uterus and IGF-IR is expressed in all cell types of the uterus, aiding in maintenance of gland development and proliferation [Taylor *et al.*, 2001].

In the developing mouse mammary epithelium, IGF-IR is needed for duct development [Kleinberg, 2000]. In this situation, GH activates GHR in the mammary stroma which induces stromal IGF-I expression to act on IGF-IR in the epithelium. Both IGF-I and -II serve as paracrine growth factors during uterine epithelial morphogenesis [for review, see Taylor *et al.*, 2001].

Presence of insulin-like binding proteins (IGFBPs) can either inhibit or enhance IGF activity and function independent of the IGFs [for review see Rosenzweig, 2004]. There are currently six known IGFBPs, which individually can have different tissue distribution, binding affinity for the IGFs, and tissue-specific functions [Cerro and Pintar, 1997; Wang and Chard, 1999; for review see Rosenzweig, 2004]. It is likely that IGFBPs function close to their sites of synthesis in an autocrine or paracrine manner [Cerro and Pintar, 1997].

Cerro and Pintar [1997] localized IGFBPs in the cycling and pregnant rat uterus and placenta with *in situ* hybridization. In the cycling rat, they detected IGFBP-1 in the deep endometrial glands, and expression was essentially absent in the LE and superficial glands near the lumen. Both IGFBP-1 and -2 possess a short tri-peptide segment that contains the sequence Arg-Gly-Asp (RGD peptide). The RGD peptide is associated with cell adhesion by localizing to the ECM and interacting with β1-integrin cell surface receptors and fibronectin. It is postulated that IGFBP-1 can promote cell motility by hindering fibronectin-integrin binding [Cerro and Pintar, 1997].

Growth factors may also be involved in the epithelial-mesenchymal interactions by signaling through ECM molecules [Sharpe and Ferguson, 1988]. Growth factors can also have opposing effects on the epithelium and mesenchyme. In the mesenchyme, TGF-β can promote the synthesis of ECM molecules; whereas in the epithelium, it can promote the synthesis of cell adhesion molecule receptors [for review, see Sharpe and Ferguson, 1988]. In essence, one growth factor can create a system that allows for

epithelial-mesenchymal interactions through the ECM and receptors [Sharpe and Ferguson, 1988].

Interactive biochemical communication factors and receptors

Regulation of uterine growth in is independent of ovarian steroids from birth to PND 60 [Wu and Dziuk, 1988; Spencer *et al.*, 1993a]. Ovariectomy (OVX) at PND 20 and PND 60 did not influence uterine length, weight, or diameter [Wu and Dzuik, 1988]. Tarleton *et al*. [1998] indicated that not only is uterine growth in the neonate pig independent of the ovary up to PND 60, but uterine adenogenesis is also not inhibited before PND 120 in OVX gilts. These results are similar to those reported in the neonatal ovine uterus [Bartol *et al.*, 1988b; Ott *et al.*, 1998] which suggests endogenous estrogens may be involved in branching morphogenesis, but not differentiation of the uterus. In addition to the role of endogenous, non-ovarian estrogens, expression of estrogen receptor alpha (ERα)-positive epithelial cells in GE of budding and proliferating uterine glands of sheep have been shown to be required for uterine gland development [Tarleton *et al*., 1998].

Estrogen

Estrogens regulate growth, differentiation, and function of many reproductive tissues. Estrogens are involved in the proliferation of cells and can modify cell characteristics by inducing growth factors and their respective receptors [Katzenellenbogen, 1996]. Many physiological processes that are tissue and organ specific, including tissue growth, differentiation, protein synthesis, and secretion are regulated through estrogen [Korach, 1994; Katzenellenbogen, 1996].

Spencer and coworkers [1993b] treated neonatal gilts with estradiol-17β valerate (EV) for 7 days prior to hysterectomy on PND 7, 14, or 49. Periods of EV exposure were selected to include the 1) infantile period which is correlated with the appearance or

initiation of uterine gland development from birth through PND 7, 2) proliferative period from PND 7–14 when there is intense glandular DNA synthesis, and 3) growth period after PND 14 when endometrial morphogenetic activity declines and the uterine histoarchitecture becomes stabilized. Uteri from the treated animals displayed increased endometrial thickness at PND 7 and 14, as well as an increase in myometrial thickness at PND 49. Distribution of uterine glands was apparent as they were less dense and less tightly coiled when compared to control animals at PND 49. The uterotropic effects of estrogen were more apparent with treatment after PND 14, when uterine growth is typically the greatest.

Responses of the neonatal uterus to exogenous estrogen imply an age-related sensitivity to the steroid in uterine tissues. Spencer and coworkers [1993b] suggest these morphogenetic responses may be an indication that 1) estrogen-sensitive cell populations develop first in the endometrium, 2) estrogen-induced abnormalities in the proportion of epithelium to stroma effect later uterine development, and 3) uterine tissues are responsive to estrogen. These researchers demonstrated that EV interrupts normal neonatal uterine developmental patterns based on exposure to estrogen during the infantile, proliferative, or growth period of uterine morphogenesis.

Antiestrogens are capable of antagonizing the effects of estrogen by binding to the ER without activating the receptor [Katzenellenbogen, 1996]. In cases of ER-containing breast cancer, antiestrogens are effectively able to suppress metastatic activity and cellular proliferation. There are two types of antiestrogens 1) Type I which are partial agonists/antagonists and 2) Type II which are complete/pure antagonists. Antiestrogens can be either steroid or non-steroid compounds. Actions of antiestrogens competitively bind ER then modify the ER structure so the receptor cannot effectively activate gene transcription [Katzenellenbogen, 1996].

Treatment of rats with antiestrogen tamoxifen at different stages of neonatal development has profound effects on uterine differentiation, dependent upon time and dose of administration. Branham and coworkers [1985] treated rats at three different stages of postnatal development: 1) neonatal from PND 1-5, 2) infantile from PND 10-14, and 3) immature from PND 20-24. Uterine weight gain was not affected by early exposure to antiestrogen during the neonatal stage, but uterine gland development was inhibited. Tamoxifen treatment during the infantile stage increased uterine weight while the number of glands was decreased, and persisted through maturation. Exposure to tamoxifen from PND 20-24 caused an increase in uterine weight, but had no effect on number of uterine glands. These effects may be due to nuclear ER binding of the antiestrogen for an extended period of time, resulting in a short-term inhibition of gland development. However, disruption of gland development persists through maturation indicating permanent actions of antiestrogen on the developing rat uterus [Branham *et al.*, 1985].

Estrogen Receptor

Estrogen receptors function as ligand-inducible transcription factors to mediate the effects of estradiol, its natural ligand [Couse *et al.*, 1995; Katzenellenbogen, 1996]. The age-specific effects of estrogen on uterine gland development are likely due to estrogen-induced, negative regulation of ERα expression [Gray *et al.*, 2001b]. Tarleton and coworkers [1998] characterized the development of ERα expression in the neonatal pig endometrium during the first 120 PND. Age-related changes were observed with immunohistochemical detection of ERα protein in the GE, LE, and stroma. Results indicate ERα-negative cell populations in the neonate porcine uterus at birth. By PND 15, GE showed intense ERα staining with minimal staining in the LE. Nuclear ERα staining became more intense in the GE of tissues from PND 30, 60, 90, and 120 while

LE ERα staining remained weak. Stromal ERα staining also steadily increased from PND 15 to PND 120. Essentially, endometrial ERα expression patterns change positively in relation to age. The same expression patterns were observed in OVX gilts, reinforcing the suggestion that neonatal uterine growth and development is ovary-independent from birth to PND 60. Moreover, these immunohistochemical findings indicate that ER-positive expression appears first in the GE and stroma, then in LE after PND 30.

Tarleton and coworkers [1998] suggested that in the neonatal pig uterus stromal ERα are necessary for endometrial cell proliferation, epithelial and stromal ERα are essential for morphogenesis and cytodifferentiation, and together these processes allow for endometrial growth and functional phenotypical organization of a mature uterus. Furthermore, cellular changes from ERα-negative to ERα-positive is an indication of GE differentiation of in the neonate pig uterus [Tarleton *et al.*, 1999]. The results of Tarleton and coworkers [1998] in conjunction with the patterns of increased DNA synthesis in GE, decrease in LE [Spencer *et al.*, 1993a], indicate a spaciotemporal relation to the emergence of uterine glands. These developmental relationships imply that ERα is needed for normal early postnatal uterine growth and adenogenesis in the pig, but is estrogen independent [Tarleton *et al.*, 1998]. Early cellular growth via ERα may be through stromal secretion of growth factors such as IGF-I and EGF [Cooke *et al.*, 1998].

Estrogen Receptor Knockout Model

Lubahn and coworkers [1993] disrupted ERα gene expression with homologous recombination to generate mice without functional ERα. Offspring homozygous for the ERα disruption are known as ERα knockout (αERKO) mice and are functionally ERα-negative. Females that exhibit αERKO are healthy but fail to develop a functional uterus. Nonetheless, the uteri do express all of the typical cell types at lower ratios,

including fewer gland numbers. This response is likely mediated through alternative regulatory pathways such as the stromal-derived growth factors IGF-I, EGF, and TGFα [for review, see Gray *et al.*, 2001b].

Couse and coworkers [1995] studied the estrogen insensitivity of ERKO female mice. They showed that estradiol binds to the uterus of ERKO females at 3% of wild type females, while no binding was detected in other ERKO tissues such as the brain, kidney, or liver. Furthermore, serum levels of estradiol were elevated in ERKO mice when compared to wild type mice, due to the absence of ER. Data from both Lubahn and coworkers [1993], and Couse and coworkers [1995] suggest a critical function of ERα for normal growth and development of the uterus, necessary for normal fertility in female mice. Female ERKO mice are infertile as they exhibited abnormal ovaries with cystic and hemorrhagic follicles, while all major cell types were present in the uterus, but were less abundant [Lubahn *et al*., 1993].

Tarleton and coworkers [1999] treated neonatal gilts with either an estrogen agonist (EV) or antiestrogen (ICI 182,780), which is a type II estrogen antagonist [Katzenellenbogen, 1996] to determine whether ERα expression is involved in neonatal pig uterine adenogenesis by inhibiting ER function. Gilts were treated from birth until PND 13 or from PND 7 until PND 13 with both compounds. Results indicated that early neonatal exposure to ER antagonist prior to ER-positive expression caused antiadenotrophic effects. Exposure to ICI from birth did not reduce endometrial thickness, but stromal cell density increased in the shallow stratum compactum, as well as adenogenesis was inhibited, when compared to control animals. Treatment with the ICI compound from PND 7 to PND 13 (the time-period in which glands are normally proliferating) did not decrease the depth of glandular penetration, but did decrease the total endometrial thickness by influencing the organization in the stroma. Conclusions of

this study imply that an activated ER system is necessary for normal uterine adenogenesis in the pig [Tarleton *et al.*, 1999].

An operational ERα system may strengthen target cell responsiveness to uterotropic growth factors. The ER-positive phenotype in the neonatal uterus may dictate the degree of responsiveness to local uterotrophic factors that affect uterine growth and endometrial maturation via estrogen-independent, membrane-initiated, ER-coupled pathways [Tarleton *et al.*, 1998].

2.4 Regulation of Porcine Uterine Gland Function

Secretory activity of the uterine glands during the estrous cycle in the pig is restricted to the mid to late luteal phase. The presence of the conceptuses during pregnancy then influence whether additional energy will be used for endometrial secretions [Bazer *et al.*, 1984]. During early pregnancy, conceptuses migrate from the oviducts into the uterine horns about 60-72 hours post-estrus [Dhindsa *et al*., 1967]. Once conceptuses develop to the blastocyst stage around Day 5 of gestation, they begin to hatch from the zona pellucida on Day 8. Prior to attachment to the uterine surface, conceptuses undergo a distinct morphological transformation from spherical (3 to 10 mm) to tubular (10 to 50 mm) to filamentous (>100mm) morphology between Days 10 to 13 of gestation [Perry and Rowlands, 1962]. Rapid trophoblast elongation throughout the uterine horns functions to increase placental surface area for maximal nutrient uptake for the conceptus and stimulation of the uterine luminal surface with estrogen. Geisert and coworkers [1982] indicated that recoverable estrogens from pregnant uterine flushings were correlated with stage of conceptus development. Increased uterine content of conceptus estrogen following trophoblastic elongation modifies endometrial $PGF_{2\alpha}$ movement so that its secretion remains exocrine and sequestered in

the uterine lumen [Bazer *et al.*, 1984]. Uterine luminal retention of $PGF_{2\alpha}$ prevents its entry into the uterine venous drainage, thus blocking the trigger to luteolysis [Bazer *et al.*, 1984; Geisert *et al.*, 1994]. Peripheral plasma estrogen levels appear to be unchanged during this time, but estradiol concentrations are greater in the utero-ovarian vein plasma and uterine flushings [Zavy *et al*., 1980]. Concentrations of $PGF_{2\alpha}$ in utero-ovarian vein do not change in early pregnancy, unlike Days 13 and 17 of the estrous cycle which increased release of endometrial $PGF_{2\alpha}$ cause luteolysis. In response to conceptus estrogens and secretions, CL are maintained and progesterone release maintained. Therefore, estrogen is the proposed maternal recognition of pregnancy signal in pigs [Geisert *et al.*, 1982c].

Effects of estrogen and progesterone upon the porcine uterus are regulated by interaction with their receptors, ER and PR [Geisert *et al.*, 1993; Geisert *et al.*, 1994]. Indeed, survival of conceptuses during early pregnancy is dependent upon conceptus estrogen synthesis to stimulate endometrial ER. Endometrial ER expression changes during the estrous cycle and early pregnancy [Geisert *et al.*, 1993]. During the follicular phase of the estrous cycle, ER is localized to the surface and glandular epithelium, and stroma. Once ovulation occurs, stromal ER expression is undetectable. Loss of the stromal ER is likely a result of progesterone-dependent inhibition during pregnancy. Endometrial ER is expressed differentially in tissue types after Day 12 of the estrous cycle as glandular ER is decreased, but ER, although decreased, persists in the surface epithelium. Surface endometrial ER at Days 10 and 12 of the estrous cycle allows conceptuses to influence the uterus via interaction between conceptus estrogen secretion and endometrial ER [Geisert *et al.*, 1993], so that pregnancy can be successfully established [Geisert *et al.*, 1994]. During early pregnancy, endometrial ER protein, mRNA synthesis and surface epithelium ER are maximal on Day 10 to 12

[Geisert *et al*., 1993]. There is an acute increase in conceptus estrogen synthesis during the period of rapid trophoblast elongation [Geisert *et al.*, 1982c] followed by a second prolonged increase of conceptus estrogen from Day 15 to 30 of gestation which provides for maintenance of CL beyond Day 30 of gestation [Geisert *et al.*, 1993].

The initiation of progesterone-induced secretory gene expression is dependent upon PR expression. Geisert and coworkers [1994] immunologically localized PR expression throughout the estrous cycle and early pregnancy in the pig. These researchers indicated that cellular PR was highest in the endometrium on Day 0 and 5 of the estrous cycle, then decreased by Day 10. Immunological staining was greatest in the surface and GE on Day 5 of the estrous cycle, then was undetectable by Day 12. However, PR was detected at Day 10 in deep GE. Stromal PR was detected throughout the cycle, becoming more intense over time until Day 18, and maintained throughout early pregnancy. The decrease in epithelial PR from Day 5 to 15 in the estrous cycle is likely a progesterone-induced down-regulation of PR [Geisert *et al.*, 1994; Gray *et al.*, 2001b].

2.5 Endometrial Secretions During the Estrous Cycle and Early Pregnancy

Histotroph, also known as uterine milk, provides nutrients to the developing conceptus. Species in which conceptuses form a noninvasive type of placental attachment, including the pig, do not come into direct contact with maternal blood supply so an alternative source of early nutrition is required [Roberts *et al.*, 1993]. Pig conceptuses do not complete placental attachment until around Day 18 of pregnancy, so nutrients via histotroph are crucial for conceptus vitality [Geisert *et al.*, 1982a]. A large assortment of endometrial proteins are secreted in response to progesterone [Roberts *et al.*, 1993]. Endometrial epithelial cell secretions are released into the uterine lumen to

supply developing conceptuses with necessary nutrition for survival and prevent regression of the CL in order to establish an epitheliochorial placentation [Geisert *et al.*, 1982a].

Corner [1921] described the changes in the mature sow uterus throughout the estrous cycle and early pregnancy. He postulated that the secretions observed during the first 8 to 10 days of pregnancy, when embryos are spherical in shape, are necessary for "flotation of the delicate embryonic vesicles" to assist intrauterine migration and spacing. Fortunately, based on current literature, the roles of the uterine secretions are now better understood. Closer observation indicates that these secretory products serve as enzymes, transport molecules, and possibly regulate genetic activity [Bazer, 1975].

Patterns of uterine protein secretions are indicative of stage of the uterine microenvironment during preimplantation [Beier, 2000] and change quantitatively and qualitatively throughout the estrous cycle [Bazer, 1975]. Based on these patterns, uterine receptivity of attaching blastocysts can be predicted. Alteration of the uterine secretion patterns will result in an unreceptive environment of the uterus for conceptuses. Administration of estradiol benzoate (EB) to rabbits 6 and 20 h post insemination caused a delay in uterine secretory patterns, resulting in total failure of blastocyst implantation [Beier, 2000]. When pregnant gilts were administered EV on Days 9 and 10, plasma progesterone was not changed and viable filamentous conceptuses were present on Day 12 and 14, but were degenerated by Day 16 [Morgan *et al*., 1987]. However, pseudopregnancy can be induced in cycling gilts by administration of exogenous estradiol from Day 11 to 15 [Geisert *et al*., 1987]. This early exposure to EV leads to an early release of calcium, protein, and uteroferrin into the uterine lumen [Morgan *et al*., 1987]. Advancing the uterine secretions in pregnant gilts disrupts the temporal relationship between maternal endometrium and developing

conceptuses. A synchronized uterine environment of secretory patterns is necessary for successful conceptus development [Beier, 2000].

Bazer [1975] stated that the changes in uterine protein secretions are related to three significant physiological events: 1) they are secreted during the luteal phase when plasma progesterone concentrations are maximum then decrease with decrease in plasma progesterone, 2) changes take place when conceptuses begin to rapidly elongate, 3) and when the CL begin to regress in cyclic animals on Day 16.

Steroid hormones are responsible for the regulation of porcine uterine protein secretions. Ovariectomized gilts treated with progesterone have an increased amount of recoverable protein from luminal fluid, indicating responsiveness of endometrium to progesterone [Knight *et al*., 1973]. As expected, the total recoverable protein correlates with the number of CL [Knight *et al*., 1973]. Bazer [1975] concluded progesterone is the primary regulator for the synthesis and/or secretion of uterine proteins in the pig.

In metestrus, uterine glands of the mature, open gilt change from slightly branched to more coiled [Sinowatz and Friese, 1983]. The neck and middle part of the glands begin to secrete histotroph in early diestrus. Secretions are apparent at the distal ends of glands near the end of diestrus, then begin to decline in proestrus. Uterine cells also undergo changes throughout the estrous cycle, corresponding with endometrial secretions [Sinowatz and Friese, 1983].

In early pregnancy, endometrial secretions are thought to have a paracrine effect on the trophoblast [Bell, 1988] and are essential for conceptus development beyond the early blastocyst stage [Bazer, 1975]. Pig conceptuses begin to produce estrogen at the 10 mm late spherical stage (around 11.5 days) which may be the trigger for the endometrium to begin secretory release [Geisert *et al.*, 1982a; Bazer and Roberts, 1983]. This period of conceptus estrogen production is at the same time that the maternal recognition of pregnancy occurs and is just prior to conceptus elongation

[Geisert *et al.*, 1982a]. Conceptus estrogen may function to induce endometrial histotroph secretion as a nutrient source. This is evident from uterine flushing from pregnant gilts in which there was a change in calcium, protein, PGF, and PGE patterns [Geisert *et al.*, 1982a]. Conceptus synthesis of estrogen then decreases on Day 13 and 14, which is evident by continually increased recoverable protein in uterine flushings [Geisert *et al.*, 1982a; Geisert *et al.*, 1990]. Geisert and coworkers [1982a] concluded that the role of conceptus estrogen on Day 12 of pregnancy is for the initial release of specific uterine proteins then later to adjust the uterine protein synthesis and/or secretion. There is a second surge of conceptus estrogen synthesis after Day 14, which continues to Day 30 of gestation. The biphasic release of conceptus estrogen is involved in the timing of uterine secretions and $PGF_{2\alpha}$ movement from endocrine to exocrine control such that $PGF_{2\alpha}$ is sequestered in the uterine lumen and cannot reach the CL via uterine vasculature [Geisert *et al.*, 1990]

Secreted Proteins

Changes in protein secretion are dependent on the hormonal environment and histological changes throughout the reproductive cycle [Bell, 1988]. Uteroferrin is detected in pregnant uterine flushings while tubular and Day 12 filamentous blastocysts are present [Buhi *et al*., 1979], correlated with initiation of conceptus estrogen production [Geisert *et al.*, 1982a]. Uteroferrin, previously known as purple acid phosphatase (PAP), is induced by progesterone and has a high affinity for iron for which it functions to transport iron from the maternal endometrium to the conceptus [Bazer and Roberts, 1983; Bazer *et al.*, 1984]. Uteroferrin is the most abundant glycoprotein synthesized and secreted by the GE, accounting for about 15% of uterine polypeptide secretions [Clawitter *et al.*, 1990]. Uteroferrin is synthesized by GE and secreted into the uterine

lumen on Days 9-13 of the estrous cycle, then begins to decline around Day 14 [Bazer *et al.*, 1984].

Retinol binding protein (RBP) is a major constituent of histotroph in which production is progesterone-dependant [Clawitter *et al.*, 1990]. It is responsible for the transport of retinol in the form of vitamin A to conceptuses [Roberts *et al.*, 1993]. Around Day 12 of pregnancy, retinol rapidly increases 10 to 50-fold and large amounts of RBP mRNA are detected in the endometrium. This dramatic increase in retinol is likely due to inability of the uterus to store retinol, therefore providing an immediate supply to meet conceptus requirements for trophoblast elongation [Trout *et al.*, 1992; Roberts *et al.*, 1993].

Lysozyme is a minor component of uterine flushings. It is responsive to progesterone [Roberts *et al*., 1976], but disproportionate to the amount of protein released [Hansen *et al*., 1985]. As a result, it is uncertain the effect progesterone has on lysozyme secretion. More recent data from postpartum mares indicate increased uterine lysozyme concentration may be a sensitive indicator of endometrial inflammation [Reilas and Katila, 2002]. In the human, lysozyme mRNA is upregulated in the regenerating crypt base epithelial cells of colonic adenocarcinoma [Yuen *et al.*, 1998]. These patterns of lysozyme mRNA and protein expression of different mucosal tissues may be indicators of local immune response to prevent bacterial infection [Yuen *et al*., 1998].

Plasmin/trypsin inhibitor (PI), a uterine Kunitz protease inhibitor, has been identified in uterine secretions during early pregnancy [Fazleabas *et al*., 1982]. This inhibitor is small and acts to impede actions of plasmin, trypsin, and possibly other serine proteinases by limiting damage from release of conceptus proteolytic enzymes [Roberts *et al.*, 1993]. Synthesis and secretion of PI is influenced by progesterone, but estrogen will work synergistically with progesterone to further control PI [Simmen and Simmen, 1990].

Lumenal IGF-I concentrations change during the estrous cycle and early pregnancy. The highest uterine luminal content of IGF-I is on Day 10 and 12 which is at the period of conceptus estrogen synthesis. IGF-I may function in a paracrine manner during conceptus development since the uterus synthesizes the ligand and the preimplantation conceptus expresses IGF-IR. IGF gene expression in the uterus can be divided into two stages: 1) during conceptus elongation when levels of IGF-I mRNA are high, IGF-II mRNA levels are low, and IGFBP-3 mRNA levels are low to moderate levels and 2) during fetal growth when concentrations of IGF-II and IGFBP-3 mRNA are high [Simmen and Simmen, 1990].

Other progesterone-responsive proteins secreted in uterine histotroph include basic glycoproteins that are family members of the serpin superfamily [Roberts *et al.*, 1993], which is a family of serine proteinase inhibitors that are similar in amino acid sequence and method of inhibition, but differ in function [Silverman *et al.*, 2001]. There is also a variety of additional proteins including leucine aminopeptidase, glucose-phosphate isomerase, beta-glycoprotein (β-glycoprotein) fraction [Bazer, 1975] and others that are unidentified [Roberts *et al.*, 1993].

2.6 Statement of the Problem

The dramatic changes that take place throughout the development of the neonatal porcine uterus have been proven necessary for later reproductive success. Formation of functional uterine glands is a postnatal event in pigs, beginning at birth and rapidly completing to functional maturity by 120 days. The morphological changes have been characterized and are regulated by several factors. Globally, uterine glands are essential for the synthesis and secretion of histotroph to support early conceptus nutritive requirements. Interruption of this developmental process is detrimental for successive reproduction.

The complete transcription profile involved in neonatal uterine adenogenesis is unknown at present. Therefore, the objective of this study was to identify differentially expressed genes involved in uterine gland development through comparison of three timepoints in postnatal growth.

2.7 Approach

Suppression subtractive hybridization (SSH) is a method to compare gene expression profiles between various stages of development. In order characterize changes in neonatal uterine gland development, SSH was used to perform a time-point analysis for the transcript profiles at three stages: PND 0 when only shallow epithelial depressions can be observed, PND 28 when glandular branching morphogenesis begins, and Day 56 when endometrial glands are well established.

Chapter 3: MATERIALS AND METHODS

3.1 Neonatal Uteri Collection

Research conducted was in accordance with and approved by the Oklahoma State Institutional Animal Care and Use Committee. Cyclic, white gilts were observed for estrus twice daily using intact boars. Females were allowed to mate naturally at the onset of the first estrus behavior and again 24 hours later. Gestation was carried out to term and day of parturition recorded as postnatal day (PND) 0. Gilts from each litter were randomly assigned to a PND group: PND 0, 14, 28, 42, or 56. For each respective PND, complete, intact uteri were collected from euthanized neonatal gilts. Neonatal gilts were anesthetized with halothane vapor then euthanized by heart-puncture with solution of saturated KCl. The body cavity was opened, the uterus trimmed below the cervix and uterine horns removed. Uteri were trimmed of supporting connective tissue, then snap-frozen in liquid nitrogen and stored at -80^{O}C until RNA extraction.

3.2 Total RNA Extraction

Total RNA was extracted from individual uteri at each PND (0, 14, 28, 42, and 56) using TRIzol Reagent (Invitrogen, Carlsbad, CA). Approximately 250 mg of whole uterine tissue was homogenized in 2.5 ml of TRIzol reagent using a Virtishear homogenizer (Virtis Co. Inc., Gardiner, NY) in a 15 ml conical polypropylene tube. Then

500 µl of chloroform was added, the mixture shaken, and centrifuged at 5,000 x g for 30 min at 4^{O}C. The aqueous phase was recovered and 2-propanol added to precipitate total RNA at -20^{O}C overnight. The following day, samples were centrifuged at 5,000 x g for 20 min at 4^{O}C to pellet total RNA and the supernatant was discarded. The pellet was washed in 80% ethanol, lightly vortexed, and centrifuged again at 5,000 x g for 10 min at 4^{O}C. Ethanol was poured off and the RNA pellet was allowed to air-dry for 10 min. Samples were then suspended in 120 µl nuclease-free H_2O and stored at -80^{O}C until use.

Total RNA concentration was determined using a LambdaBio spectrophotometer (PerkinElmer, Wellesley, MA) to determine absorbance at 260 nm and 280 nm (A_{260}:A_{280}). All uterine total RNA samples had a A_{260}:A_{280} of 2.0 or greater. One µl of total RNA from each sample was mixed with 8 µl of nuclease-free H_2O and 1 µl of 10 x gel loading buffer to bring the sample volume to 10 µl. Products were loaded into a 1% agarose gel and allowed to migrate and separate through the agarose at 115 volts (V) for 45 min. The agarose gel was stained in ethidium bromide (EtBr) solution (5 µg/µl) for 5 min to detect nucleic acids, then rinsed in distilled H_2O and imaged using ultraviolet (UV) light and Kodak 1D Imaging Software.

3.3 Isolation of polyA^{+} RNA

Poly A^{+} RNA was isolated from previously purified total RNA using an Ambion® (Austin, TX) Poly(A)Purist™ RNA isolation kit. The absorbance at 260 nm was determined and 100 µg of total RNA from the four samples from each day (PND 0, 28, or 56) were pooled to bring a final concentration of 400 µg per PND. Volumes were brought up to 250 µl with sterile distilled nuclease-free H_2O. An equal volume of 2X

binding solution was added and then mixed. Each pooled RNA sample was added to oligo(dT) cellulose and mixed by inverting to resuspend the solution.

The reaction was heated for 5 min at 75^{O}C to denature secondary structures then allowed to shake at RT on a platform shaker for 1 h to allow PolyA^{+} to bind to the oligo(dT) cellulose. The cellulose was pelleted at 10,000 x g for 3 min and the supernatant removed. Cellulose pellet was washed twice with 500 µl wash solution 1 by placing the mixture on a spin column seated in a 2 ml centrifuge tube and centrifuging at 10,000 x g for 3 min. The filtrate was discarded and the mixture washed 3X with 500 µl wash solution 2 by centrifuging at 10,000 x g for 3 min. PolyA^{+} RNA was eluted in 200 µl of RNA storage solution by spinning at 10,000 x g for 2 min, adding an additional 200 µl of RNA storage solution, and repeating. Precipitation was carried out overnight at -20^{O}C.

Messenger RNA was recovered by centrifugation at 10,000 x g for 30 min at 4^{O}C. The supernatant was removed and the mRNA pellet washed with 70% ethanol, centrifuged for 10 min at 4^{O}C and residual ethanol removed. The pellet was air dried then suspended in 7 µl RNA storage solution. Concentration of mRNA was determined spectrophotometrically. RNA was stored at -80^{O}C until use.

3.4 Suppression Subtractive Hybridization

Suppression subtractive hybridization profiles differentially expressed genes. Gene expression differences in neonatal uteri were evaluated with a Clontech™ (Palo Alto, CA) PCR Select cDNA subtraction kit. Two different forward and reverse subtractions were performed to compare gene expression during uterine gland development between PND 0 and 28, and between PND 28 and 56. Each SSH

comparison utilized 2 µg of pooled PND mRNA. The specific transcripts identified were found in the tester population, while the reference cDNA was the driver. For the PND 0 vs. PND 28 comparison forward subtraction, PND 0 was the tester and PND 28 the driver. For the reverse subtraction, PND 28 was the tester and PND 0 the driver. Likewise in the PND 28 vs. PND 56 comparison, PND 28 was the tester and PND 56 the driver in the forward subtraction. The tester for the reverse subtraction was PND 56 and the driver PND 28.

First Strand Synthesis. For each experimental and tester PND and control PolyA$^+$ RNA (from human skeletal muscle), 2µg of mRNA was mixed with 1 µl of cDNA synthesis primer (10µM) and brought to a final reaction volume of 5 µl with 0.1% DEPC-treated H_2O in a 0.2 ml PCR tube. The reaction was placed in a MJ Research PTC-100 (Waltham, MA) and heated to 70^oC for 2 min, placed on ice for 2 min, briefly centrifuged, and then a master mix for the first strand synthesis was prepared. For each reaction the following was added: 2 µl of 5X first strand synthesis buffer (250 mM Tris HCl [pH 8.5], 40 mM $MgCl_2$, 150 mM KCl, 5 mM dithiothreitol [DTT]), 1 µl of 10 mM dNTP's, 1 µl DEPC H_2O, and 1 µl of Avian Myeloblastosis Virus (AMV) reverse transcriptase (20 units/µl). Each reaction was mixed, briefly centrifuged, then placed in a PTC-100 for 1 h at 42^oC. Afterwards, the reaction was placed on ice while the master mix for second-strand synthesis was prepared.

Second-Strand cDNA Synthesis. Seventy µl of second-strand synthesis master mix containing 48.4 µl DEPC H_2O, 16 µl 5X second-strand synthesis buffer (500 mM KCl, 50 mM ammonium sulfate, 25 mM $McCl_2$, 0.75 mM β-NAD, 100 mM Tris-HCl [pH 7.5], 0.25 mg/ml BSA), 1.6 µl 10 mM dNTP's, and 4 µl 20X second-strand enzyme cocktail (DNA polymerase I [6 U/µl], RNase H [0.25 U/µl], E. coli DNA ligase [1.2 U/µl])

was added to each first strand synthesis reaction. The mixture was lightly mixed, centrifuged, and placed in a PTC-100 for 2 h at 16^{o}C. Six units (2 µl) of T4 DNA polymerase was added to the reaction and incubated at 16^{o}C for an additional 30 min. Products were transferred to a 1.5 ml tube then extracted by adding 100 µl phenol:chloroform:isoamyl alcohol (25:24:1), vortexing, and centrifuging at 14,000 rpm for 10 min at rt. The top aqueous layer was removed and the previous step repeated using 20 µl of phenol:chloroform:isoamyl alcohol. In a new 1.5 ml tube, 100 µl chloroform:isoamyl alcohol (24:1) was added to the aqueous layer, vortexed and centrifuged at 14,000 rpm for 10 min.

Again, the top aqueous layer was recovered and 50 µl of 4M ammonium acetate (NH_4OAc) solution and 375 µl of 100% ethanol (EtOH) were added. Precipitation of cDNAs was carried out by vortexing the mixture and centrifuging at 14,000 rpm for 20 min. The supernatant was removed, cDNA pellet washed with 500 µl of 70% EtOH, and centrifuged for 10 min. Two additional 70% EtOH washes were performed. The remaining pellet was air dried for 10 min, dissolved in 50 µl of DEPC H_2O. Six µl of the second strand synthesis were set aside for analysis by gel electrophoresis. All products were stored at -20^{o}C until later use.

Rsa I *Digestion*. After generation of cDNA for each tester and driver, the products were blunt-ended into fragments for optimal subtraction and adaptor ligation. To 43.5 µl of the second-strand synthesis, 5 µl of 10X *Rsa* I restriction buffer (100 mM Bis Tris Propane HCl [pH 7.0], 100 mM $MgCl_2$, 1 mM DTT) and 1.5 µl of *Rsa* I (10 U/µl) were added. The mixture was lightly mixed and incubated at 37^{o}C in a PTC-100 for 3 h. Five µl of the digestion were set aside for later analysis by gel electrophoresis. The reaction was stopped by adding 2.5 µl of 20X EDTA/glycogen mix (0.2 M EDTA, 1 mg/ml

glycogen), then purified by adding 50 µl phenol:chloroform:isoamyl alcohol (25:24:1) and centrifuging for 10 min at 14,000 rpm. The top aqueous phase was recovered and placed into a new microcentrifuge tube. The previous steps were repeated using an additional 20 µl of phenol:chloroform:isoamyl alcohol and the aqueous phase recovered. Purification was continued by adding 50 µl of chloroform:isoamyl alcohol (24:1), centrifuging for 10 min at 14,000 rpm, and recovering the aqueous phase.

Precipitation of digested products was initiated by adding 35 µl of 4M ammonium acetate (NH_4OAc) solution and 262.5 µl of 100% EtOH. Reaction was mixed and centrifuged for 20 min at 14,000 rpm. The supernate was removed and remaining pellet was washed by overlaying with 200 µl of 70% EtOH. The pellet was centrifuged for 5 min and the pellet was washed two additional times with 70% EtOH. The pellet was allowed to air dry for 10 min, and then dissolved in 5.5 µl of DEPC H_2O. Digested products were stored at -20^{o}C until later use. Efficiency of the digestion was determined by running 2.5 µl of the products on a 1.0% agarose gel at 115 V for 45 min, then staining in EtBr, and imaging using UV light.

Adaptor Ligation. The ligation of adaptors (Table 3.1) to each *Rsa* I digested tester was necessary for enrichment of differentially expressed sequences for each comparison. For each tester cDNA, there were three adaptor ligations: Adaptor 1, Adaptor 2R, and Unsubtracted Control. First, 1 µl of the tester cDNA was diluted into 5 µl of DEPC H_2O. Adaptor master mix was prepared for each ligation, consisting of: 3µl DEPC H_2O, 2 µl of 5X ligation buffer (250 mM Tris-HCl [pH 7.8], 50 mM $MgCl_2$, 10 mM DTT, 0.25 mg/ml BSA), and 1 µl of T4 DNA ligase (400 U/µl).

Tester cDNA adaptor ligations were set up in a 0.2 ml PCR tube and the following added: 2 µl of dilute tester cDNA, 10 µM of either Adaptor 1 (Tester 1-1) or Adaptor 2R (Tester 1-2) , and 6 µl of prepared adaptor master mix to bring the reaction

up to a total volume of 10 µl. A third ligation was prepared to serve as the unsubtracted control (Tester 1-c). Two microlters of Tester-1 was mixed with 2 µl of Tester-3 in a new 0.2 ml tube. The reactions were mixed and incubated at 16^{O}C overnight in a PTC-100.

Table 3.1. Sequences of the Clontech PCR-Select cDNA synthesis primer, adaptors, and PCR primers.

Primer	Sequence
cDNA Synthesis	5'-TTTTGTACAAGCTT$_{30}$N$_1$N-3'
Adaptor 1	5'-CTAATACGACTCACTATAGGGC TCGAGCGGCCGCCCGGGCAGGT-3'
Nested PCR 1	5'-TCGAGCGGCCGCCCGGGCAGGT-3'
Adaptor 2R	5'-CTAATACGACTCACTATAGGG CAGCGTGGTCGCGGCCGAGGT-3'
Nested PCR 2R	5'-AGCGTGGTCGCGGCCGAGGT-3'

Ligation reactions were stopped by adding 1 µl of 20X EDTA/Glycogen mix and T4 DNA ligase was inactivated by heating to 72^{O}C for five min. For each unsubtracted tester (Tester 1 and Tester 2), 1 µl was diluted into 1 ml of DEPC H_2O and the samples were stored at -20^{O}C.

Efficiency of the adaptor ligation was tested to see whether at least 25% of the cDNA's have adaptors on both ends by diluting 1 µl into 200 µl of H_2O and then PCR amplifying the adaptors. The subtraction kit provides glyceraldehyde-3-phosphate dehydrogenase (G3PDH) primers that are compatible with human, mouse, and rat cDNA. However, these primers were not useful for amplification of pig G3PDH, so efficiency was determined solely based on the control ligation reaction. A ligation analysis master mix was prepared, consisting of the following: 18.5 µl of sterile H_2O, 2.5 µl 10 x BD Advantage™ 2 (Clontech, Palo Alto, CA) PCR reaction buffer (400 mM

Tricine-KOH (pH 8.7), 150 mM KOAc, 35 mM $Mg(OAc)_2$, 37.5 µg/ml BSA, 0.05% Tween-20, 0.05% Nonidet-P40), 0.5 µl dNTP (10 mM), and 0.5 µl 50 x BD Advantage™ 2 (Clontech, Palo Alto, CA) polymerase mix (50% glycerol, 15 mM Tris HCl [pH 8.0], 75 mM KCl, 0.05 mM EDTA). The four PCR reactions were set up as described in Table 3.2. Twenty-two µl of the prepared master mix were added to each tube and briefly mixed. The reactions were placed in a PTC-100 and incubated at 75^{o}C for 5 min to extend the adaptors. The following thermal cycling parameters were then followed: 20 cycles of 94^{o}C for 30 sec, 65^{o}C for 30 sec, and 68^{o}C for 2.5 min. Five microliters of the PCR products were analyzed on a 1.5% agarose gel, stained in EtBr.

Table 3.2. Adaptor Ligation Efficiency PCR Setup.

	Tube:			
Component	**1**	**2**	**3**	**4**
Tester 1-1	1	1	-	-
Tester 1-2	-	-	1	1
G3PDH 3' Primer	1	1	1	1
G3PDH 5' Primer	-	1	-	1
PCR Primer 1	1	-	1	-
Total Volume	3	3	3	3

First Hybridization. Once adaptor ligation has been verified, tester cDNA was then hybridized in excess of driver cDNA then heat denatured to generate cDNA that can be exponentially amplified using the two new adaptors. During the first hybridization, 1.5 µl of tester (with either Adaptor 1 or Adaptor 2R) was hybridized for 8 h with 1.5 µl of *Rsa* I digested driver cDNA and 1 µl of 4X Hybridization Buffer (Clontech, Palo Alto, CA) at 68^{o}C in a PTC-100. Five different types of molecules form during this

hybridization. Three were cDNAs that cannot amplify because they either have no adaptor ligated, only one adaptor ligated, or form a self-dimer. If two molecules bind with the same adaptor primer annealing site, the molecule will only amplify linearly. The fifth type of molecule had both Adaptor 1 and Adaptor 2R annealing sites for exponential amplification.

Second Hybridization. Fresh driver was denatured at 98^{o}C for 1.5 min with 4X hybridization buffer and H_2O. Then, each tester with Adaptor 1 and Adaptor 2R were mixed together with the excess denatured driver and incubated overnight at 68^{o}C. During this step, high and low abundance cDNA sequences were equalized among each other. The following day, 200 µl of dilution buffer (20 mM HEPES-HCl [pH 8.3], 50 mM $MgCl_2$, 10 mM DTT, 0.25 mg/ml BSA) was added to each subtraction then stored at -20^{o}C overnight.

PCR Amplification. The molecules that have both primer annealing sites from the subtraction were able to be exponentially amplified during PCR. Seven PCR reactions were set up for the primary PCR: 1) forward-subtraction;, 2) forward unsubtracted control, 3) reverse-subtraction unsubtracted control, 4) reverse unsubtracted control, 5) subtracted tester control, 6) unsubtracted tester control, and 7) PCR control subtracted cDNA.

A primary PCR master mix was prepared consisting of 19.5 µl sterile H_2O, 2.5 µl of 10X BD Advantage™ 2 PCR reaction buffer, 0.5 µl of 10 mM dNTP mix, 1.0 µl 10 µM PCR Primer 1, and 0.5 mM 50X BD Advantage™ 2 cDNA Polymerase for each reaction. Primary PCR reactions were heated to 75^{o}C to extend the adaptors and create a binding site for PCR primers. Thermal cycling parameters were 27 cycles of

94^{O}C for 30 sec, 66^{O}C for 30 sec, then 72^{O}C for 1.5 min. Primary PCR products were diluted 3 µl into 27 µl DEPC H_2O.

Secondary PCR. One µl of each dilute primary PCR product was used as template cDNA for secondary PCR. The secondary PCR master mix was prepared containing 18.5 µl sterile H_2O, 2.5 µl PCR reaction buffer, 1.0 µl 10 µM nested PCR primer 1, 1 µl 10 µM nester PCR primer 2R, 0.5 µl 10 mM dNTP mix, and 0.5 µl Advantage cDNA polymerase mix for each secondary PCR reaction. Thermal cycling parameters were 12 cycles of 94^{O}C for 30 sec, 68^{O}C for 30 sec, and 72^{O}C for 1.5 min.

Primary and secondary PCR products were visualized on a 1.5% agarose gel run in 1X TEA and stained in EtBr. Each subtraction was then enriched for differentially expressed cDNA sequences. Secondary PCR products were stored at -20^{O}C until later use.

Following secondary PCR, cDNA were adenylated to stabilize each sequence. Fifteen µl of secondary PCR for each subtraction were mixed with 25 µl of chloroform:isoamyl alcohol (24:1), vortexed, and the spun for 5 min at 13,000 rpm. Ten µl of the supernate were recovered, then mixed with 1 µl of dATP (Applied Biosystems, Foster City CA), 1 µl Advantage PCR reaction buffer, and 0.5 µl AmpliTaq (Applied Biosystems, Foster City CA). The mixture was placed in a PTC-100 for 10 min at 72^{O}C. Four µl of the adenlyated secondary subtracted products were then used for ligation into vector.

3.5 Vector Cloning

Secondary PCR products were inserted into a TOPO® TA pCR4 (Invitrogen, Carlsbad, CA) cloning vector to identify sequences for each insert. Four µl of each

secondary PCR were mixed with 1 µl of salt solution (1.2 M NaCl, 0.06 M $MgCl_2$) and 1 µl of cloning vector. The reaction was incubated at RT for 30 min, then placed at 4^{o}C overnight. The following day, 2 µl of the cloning reaction were gently mixed with One Shot® TOP10 (Invitrogen, Carlsbad, CA) chemically competent *E. coli* cells. The reaction was carried out for 30 min on ice and heat shocked at 42^{o}C for 30 sec. The transformation was immediately placed on ice and 250 µl of rt S.O.C. Medium (2% tryptone, 0.5% yeast extract, 10 mM NaCl, 2.5 mM KCl, 10 mM $MgCl_2$, 10 mM $MgSO_4$, 20 mM glucose) was added. Each reaction was capped and shaken for 2 h at 37^{o}C. Fifty or 100 µl from each transformation was spread onto prewarmed selective agar plates (LB agar, 100 mg/ml carbenicillin, 18 mg/ml X-GAL, 7.2 x 10^{-5} M IPTG). Plates were placed in a 37^{o}C incubator (Fisher Scientific, Pittsburg, PA) inverted for 16 h.

Small, white colonies were picked the following day using sterile toothpicks. Each colony was streaked onto a new pre-warmed selective agar plate, placed into 2 mL of Terrific Broth (12 g Bacto® tryptone, 24 g yeast extract, 2.31 g KH_2PO_4, 12.54 g KH_2PO_4) (Fisher Scientific, Pittsburg, PA) with 100 µg/ul carbenicillin for plasmid extraction, and in 700 µl Terrific Broth with 300 µl 90% glycerol for back-up storage at -80^{o}C. Agar plates with plasmids were incubated overnight at 37^{o}C, plasmids in Terrific Broth were incubated in a shaking incubator (New Brunswick Scientific, Edison, NJ) for 16 h.

3.6 Plasmid extraction

Plasmid DNA was purified in a 96-well format using Wizard® SV 96 System (Promega, Madison, WI). Bacterial cells were pelleted by centrifuging for 15 min at 1,500 x g then pouring off the supernate and blotting upside down. Cells were

resuspended in 250 µl of resuspension solution (50 mM Tris-HCl [pH 7.5], 10 mM EDTA, 100 µg/ml RNase A), 250 µl of cell lysis solution (0.2M NaOH, 1% SDS) added, mixed, then incubated 3 min at rt. Neutralization solution (4.09 M guanidine hydrochloride, 0.759 M potassium acetate, 2.12M glacial acetic acid) was added (350 µl) and the total mixture was transferred to a prepared vacuum manifold (Promega, Madison, WI) assembled with a lysate clearing plate and a DNA binding plate (Promega, Madison, WI). Lysates were allowed to sit on plate for 1 min, and then vacuum was applied for 5 min. An additional 500 µl of neutralization solution was added to each well and vacuum was applied for 1 min.

Each well was washed with 1.0 mL of wash solution (162.8 mM potassium acetate, 27.1 mM Tris-HCl [pH 7.5], 95% EtOH), vacuum applied for 1 min, and the process repeated. The plates were dried by applying vacuum for 10 min. The vacuum manifold was dissembled to remove the DNA binding plate and then blotted on paper towels to remove residual EtOH.

The DNA binding plate was placed on the vacuum manifold, above an elution plate (Promega, Madison, WI) and 100 µl of DEPC H_2O added to each well in the binding plate. The plate was incubated for 1 min at rt, then vacuum applied for 1 min. Plasmid DNA was now eluted and ready for quantification.

Concentrations of purified plasmid cDNAs were fluorescently quantified using PicoGreen® quantitation reagent (Molecular Probes, Eugene, OR). TE Buffer (100 mM Tris-Hcl [pH 7.5], 10 mM EDTA) was diluted to 1X and a working solution of PicoGreen was prepared by making a 200X dilution. Two microliters of each purified cDNA sample was diluted in 73 µl of 1X TE Buffer then mixed with 75 µl of dilute PicoGreen reagent. A standard curve was generated using a lambda DNA standard in duplicate.

Fluorescence was quantified using a PerkinElmer (Wellesley, MA) Wallac Victor2 plate reader.

Immobilizing plasmid DNA. Plasmid DNA was denatured in a 96-well pate with 250 µl 0.5 M NaOH and 1.5 M NaCl for 10 min at rt. Meanwhile, positively charged membranes (Roche Diagnostics, Indianapolis, IN) were pre-wetted in distilled H_2O. Four separate Bio-Dotter apperati were assembled, each with one membrane. Membranes were rehydrated by adding 100 µl of denaturing solution (5 M NaCl, 0.5 M NaOH) to all 96 sample wells and gentle vacuum applied to remove the buffer. Seventy-seven microliters of denatured DNA were added to each sample well and bound to membrane with gentle vacuum. Sample wells were rinsed with 200 µl neutralization solution (1M Tris-HCl [pH 8.0], 1.5 M NaCl) and incubated at RT for 10 min, followed with gentle vacuum. All membranes were removed from each Bio-Dotter, placed on 2X SSC-soaked blotting paper, then UV-crosslinked to fix the cDNA onto membranes. All membranes were stored at 4^{o}C until use.

3.7 Differential Screening

Individual clones were confirmed for differential expression using the DIG High Prime DNA Labeling and Detection Starter Kit II (Roche Diagnostics, Indianapolis, IN). This method uses digoxygen (DIG) to label secondary PCR products from each SSH comparison, both subtracted and unsubtracted products, forward and reverse.

DIG-DNA Labeling

Four secondary PCR reactions were performed for all SSH comparisons as described above in the SSH protocol. The four individual PCR products for each comparison were combined to a total volume of 100 µl and 2.5 µl were used to determine A_{260}. Two micrograms of PCR product were digested with *Rsa* I enzyme in

20 µl volume for 1 h at 37^{o}C. The restriction digested products were purified using QIAquick PCR Purification Kit (Qiagen, Valencia, CA). Briefly, all 20 µl of the digest were mixed with 5 volumes of Buffer PB (Qiagen), mixed, then loaded onto the resin column, with 2 ml collection tube. To bind DNA, the columns were centrifuged for 60 sec at 10,000 rpm. The flow-through was recovered and passed through the column a second time. After the second binding, the flow-through was discarded. The column was placed back into the tube then washed with 750 µl Buffer PE (Qiagen) and centrifuged for 60 sec. The flow-through was discarded, then the column was spun for 1 min to remove residual ethanol. Purified DNA products were eluted in 20 µl of H_2O by centrifugation. Following purification, A_{260} was determined and 1 µg of DNA was diluted in 16 µl of H_2O as template for DIG labeling.

Template DNA was denatured by heating to 95^{o}C in a PTC-100 for 10 min, then chilled on ice. Four µl of DIG-High Prime were added to the freshly denatured template followed by hybridization with template DNA for 20 h. Hybridization reactions were stopped by heating to 65^{o}C for 10 min. The control DIG labeled DNA was serially diluted then spotted onto a positively charged nylon membrane (Roche Diagnostics, Indianapolis, IN).

Labeling was detected immunologically with an anti-digoxygen-AP conjugate. The membrane was rinsed in 20 ml maleic acid buffer (0.1 M maleic acid, 0.15 NaCl [pH 7.5]) for 2 min at RT then transferred to 30 ml blocking solution (Roche Diagnostics, Indianapolis, IN) for 30 min at rt. Membranes were sequentially transferred into 20 ml of antibody solution (anti-digoxygen-AP 75 mU/ml in blocking solution) for 30 min, twice for 15 min in 50 ml of washing buffer (0.1 M maleic acid, 0.15 NaCl [pH 7.5], 0.3% (v/v) Tween 20), then equilibrated for 5 min in 10 ml detection buffer (0.1 M Tris-HCl, 0.1 M NaCl [pH 9.5]). The membrane was then placed on a cut open Ziploc bag and 100 µl

CSPD-ready-to-use (Roche Diagnostics, Indianapolis, IN) was applied, covered with the second sheet of Ziploc, and incubated at RT for 15 min. Edges of the bag were heat-sealed and membranes were exposed to x-ray film (X-OMAT LS, Kodak, Rochester, NY) for 20 min. Film was processed automatically with an automatic x-ray film processor (Konica, Scarborogh, ME). Intensity of the spots from each labeling reaction was compared with the control spots. Amount of DIG-labeled DNA was determined and each probe was diluted to 25 ng/ml in 8 ml DIG Easy Hyb.

Hybridization

Previously prepared cDNA membranes were hybridized with the subtracted or unsubtracted cDNA DIG-labeled probes overnight to screen for differentially expressed cDNAs. First, a working solution of DIG Easy Hyb Granules (Roche Diagnostics, Indianapolis, IN) were dissolved in 64 ml sterile double distilled H_2O and stirred for 5 min at 37^{o}C. Volume of DIG Easy Hyb was determined based on membrane size at a rate of 10 ml/100 cm^2 membrane and preheated to 38^{o}C. Each membrane (4 per comparison) was placed in a roller-bottle and prehybridized for 30 min at 38^{o}C in a rotating incubator. Meanwhile, the DIG-labeled probes were denatured in a PTC-100 thermalcycler for 5 min at 95^{o}C. Each probe was then added to the pre-heated DIG Easy Hyb (3.5 ml/ 100 cm^2 membrane) and thoroughly mixed. The prehybridization buffer was recovered and replaced with the probe/hybridization mixture. All membranes were incubated overnight with rotation.

Stringency Washes. The following day, probe/hybridization mixtures were recovered and stored at -20^{o}C. Membranes were carefully removed from the roller bottle and stringency washed twice for 5 min in stringency wash 1 (2x SSC, 0.1% SDS)

at RT with constant shaking. Stringency wash 1 was replaced with stringency wash 2 (0.5x SSC, 0.1% SDS) prewarmed to 65^{o}C for two 15 min washes with constant rotation.

Immunological Detection

After stringency washes, membranes were subjected to immunological detection of DIG-labeled probes. All incubations were carried out at RT on a platform shaker. Membranes were first washed for 5 min in washing buffer, incubated for 30 min in 50 ml blocking solution, 30 min in 20 ml antibody solution, then washed twice for 15 min in washing buffer. The membranes were equilibrated for 5 min in detection buffer, transferred to an opened Ziploc bag, 1 ml CSPD ready-to-use applied, membrane covered with second sheet of Ziploc, and incubated for 5 min. Excess CSPD was squeezed out and edges of the bag were heat-sealed. Sealed membranes were then incubated for 10 min at 37^{o}C to enhance luminescence. Immunologically detected membranes were exposed to x-ray film (X-OMAT LS, Kodak, Rochester, NY) for 30-45 sec and film processed immediately. Images were saved electronically using a light box, digital camera, and Kodak 1D software.

3.8 *Eco*R I digestion

Following extraction, the plasmid cDNAs were digested with *Eco*R I to determine insert size and redundancy within each cloning reaction. A master mix for all 96 clones was prepared, and consisted of 2 µl 10X Buffer H (Promega, Madison, WI) (90 mM Tris-HCl, 10 mM $MgCL_2$, 50 mM NaCl), 0.2 µl acetylated BSA (10 µg/ul), and 0.5 µl *Eco*R I restriction enzyme (12 U/µl). One microgram of cDNA was digested and total volume was brought up to 20 µl with DEPC H_2O. Digestion was prepared in a 96-well PCR plate and placed in a PTC-100 for 4 h at 37^{o}C. Digested products were analyzed on a 1.5% agarose gel run in 1X TAE buffer and stained in EtBr.

3.9 DNA Sequencing

Sequence of plasmids that showed differential expression through differential screening were determined using a CEQ 8000 Genetic Analysis System (Beckman-Coulter, Fullerton,CA).

Clone cDNA templates were concentrated to 260 ng in 10 µl of sterile H_2O then heat denatured for 5 min at 86^{O}C in a PTC-100 and placed immediately on ice. Eight µl dye terminator cycle sequencing (DTCS) Quick Start Kit (Beckman-Coulter, Fullerton, CA) plus 2µl of sequence primer (5 µm), (either forward or reverse) were added to each denatured sample. The reactions were mixed, spun down, and then placed in a PTC-100 with the following cycling parameters: 30 cycles of 96^{O}C for 20 sec, 50^{O}C for 20 sec, 60^{O}C for 20 sec, then held at 4^{O}C.

The PCR reaction was stopped by adding 5 µl of stop solution (1.5 M NaOAc, 50 mM EDTA, 20 mg/ml glycogen). Precipitation followed by adding 60 µl of ice-cold 95% EtOH, sealing with aluminum, and centrifuging at 5,700 rpm in an Allegra™ 25 centrifuge (Beckman-Coulter, Fullerton, CA) for 10 min. Plate was turned upside down to pour off ethanol, then spun inverted at 300 rpm for 20 sec. The plate was turned right-side up, rinsed twice with 200 µl of ice-cold 70% EtOH and pelleted at 5,700 rpm and drying at 300 rpm as above. After removal of residual EtOH, the pellets were allowed to air dry for 10 min, then 40 µl of sample loading solution (Beckman-Coulter, Fullerton, CA) was added to resuspend each pellet. The mixture was overlain with 1 µl of mineral oil (Beckman-Coulter, Fullerton, CA) and placed in the CEQ 8000 for analysis.

3.10 Sequence Identity

Each sequence output from the CEQ 8000 Genetic Analysis System was identified using Basic Local Alignment Search Tool (BLAST) [Altschul *et al.*, 1990]. Sequences were first searched for vector contamination using VecScreen (National Center for Biotechnology Information) and portions of inserts with contamination were not used for BLAST.

3.11 PCR Primer Design

Primers for real-time PCR were designed using Integrated DNA Technologies (IDT) PrimerQuest^{SM}. Parameters were limited to an optimum primer size of 24 nucleotides, TM of 60^{o}C, 50% GC content, products less than 300 bp, no more than three runs of Gs, and the five nucleotides at the 3' end do not have more than two G and/or C bases. Primer pairs were designed for SPARCL1, clone PND 0 vs. PND 28 #47, and clone PND 28 vs. PND 0 #7.

3.12 Quantitative Real-Time PCR (qRT-PCR)

Transcripts for SPARCL1, clone PND 0 vs. PND 28 #47, and clone PND 28 vs. PND 0 #7 mRNA were assayed using quantitative real-time PCR (qRT-PCR) and SYBR Green I, while endogenous 18S was assayed using a fluorescent reporter. Neonatal uterine tissue from five time points in three developmental stages was assayed: infantile (PND 0), proliferative (PND 14), and growth (PND 28, 42, and 56). Amplification was conducted with an Applied Biosystems PRISM® 7500 Sequence Detection System (ABI, Foster City, CA). Total RNA from different PND uteri was assayed in duplicate at a concentration of 100 ng for amplification of each target and 18S ribosomal control.

Expression of 18S ribosomal RNA was analyzed using a one-step reverse transcription qRT-PCR Master Mix for TAMRA®-labeled probe kit (Eurogentec, Philadelphia, PA). Each reaction for TAMRA®-labeled 18S probe consisted of .0625U EuroScript reverse transcriptase (Moloney murine leukemia virus) with 0.025U RNase Inhibitor, 18S forward and reverse primers (25 nM), 18S 5' FAM, 3' TAMRA labeled probe (100 nM), and reaction buffer with dNTPs (including dUTP), Hot Goldstar DNA polymerase, $MgCl_2$ (5 mM final concentration), stabilizers, and ROX passive reference.

Amplification of target mRNA expression was detected with a one-step reverse transcription qRT-PCR for SYBR Green I (Eurogentec, Philadelphia, PA). Each target reaction final concentration consisted of 0.0625U EuroScript reverse transcriptase (Moloney murine leukemia virus) with 0.025U RNase inhibitor and reaction buffer with dNTPs, Hot GoldStar DNA Polymerase (0.025U/µl), 5 mM $MgCl_2$, SYBR Green I, ROX passive reference.

Primer Optimization and Melting CurveAnalysis

Before quantitative differences could be determined, cycling conditions were optimized and primer melting curve analysis performed. Total RNA at a 10-fold difference (50 ng and 5 ng) and a no template control (NTC) (0 ng) were analyzed in duplicate for each primer pair at 0.5 µM. Cycling parameters for the each primer melting curve analysis were: 1) initial 30 min reverse transcription at 50°C, 2) 15 min 95°C Hot GoldStar reverse transcriptase activation, 3) 40 cycles of 95°C for 15 sec, 55°C for 30 sec, 72°C 20 sec, and 4) an additional extension at 76°C for 34 sec. Cycling was followed immediately by a melting curve analysis with an initial 95°C for 15 sec, 19 min and 59 sec annealing ramp time beginning at 60°C to 95°C for a 15 sec denature.

Fluorescence data was acquired at the second extension phase and throughout the 20 min dissociation.

Melting curves were analyzed using the Dissocation Curve™ software by Applied Biosystems (Foster City, CA). Desired results were a primer set that had a higher, yet distinct, T_M than the primer-dimers formed in the NTC. The temperature between the primer dimer melting and the target melting was the temperature necessary to collect data during a real-time assay.

Quantitative RT-PCR

Cycling parameters for the each real-time SYBR Green assay were: 1) initial 30 min reverse transcription at 50^{o}C, 2) 15 min 95^{o}C Hot Start reverse transcriptase activation, 3) 40 cycles of 95^{o}C for 15 sec, 60^{o}C for 1 min, 72^{o}C 1 min, T_M for specific target for 15 sec (as determined by the melting curve analysis and which was the data acquisition step). A melting curve analysis was also performed immediately following each assay.

Results of qRT-PCR were analyzed using relative quantification and determining fold difference. Microsoft Excel® software was used to determine the difference in cycle threshold (ΔC_T) between the target cycle threshold (C_T) and the 18S RNA C_T for each uterine sample. Based on the ΔCT, the fold differences in gene transcripts were calculated using $2^{-\Delta\Delta Ct}$. To determine assay efficiency, a standard curve for each reaction plate was generated from the log of the concentration of initial RNA to the C_T and adding a linear trend line to determine the R^2-value.

3.13 Statistical Analysis

The statistical model used for this analysis tested the fixed effect of postnatal day (PND 0, 14, 28, 42, and 56). Quantitative RT-PCR ΔC_T was determined for each pig, and therefore pig was the experimental unit. Data were analyzed using PROC MIXED of the Statistical Analysis System (SAS). Significance ($P < 0.05$) was determined using probability differences of Least squares means (LSM) between postnatal days on uterine gene expression of SPARCL1, clone PND 0 vs. PND 28 #47, and clone PND 28 vs. PND 0 #7.

Chapter 4: RESULTS

4.1 Total RNA Extraction

Total RNA was extracted from whole uteri at PND 0, 14, 28, 42, and 56 (n=4/PND). Quality of RNA was high as determined both spetrophotometrically and visually on a 1.0 % agarose gel (Figure 4.1).

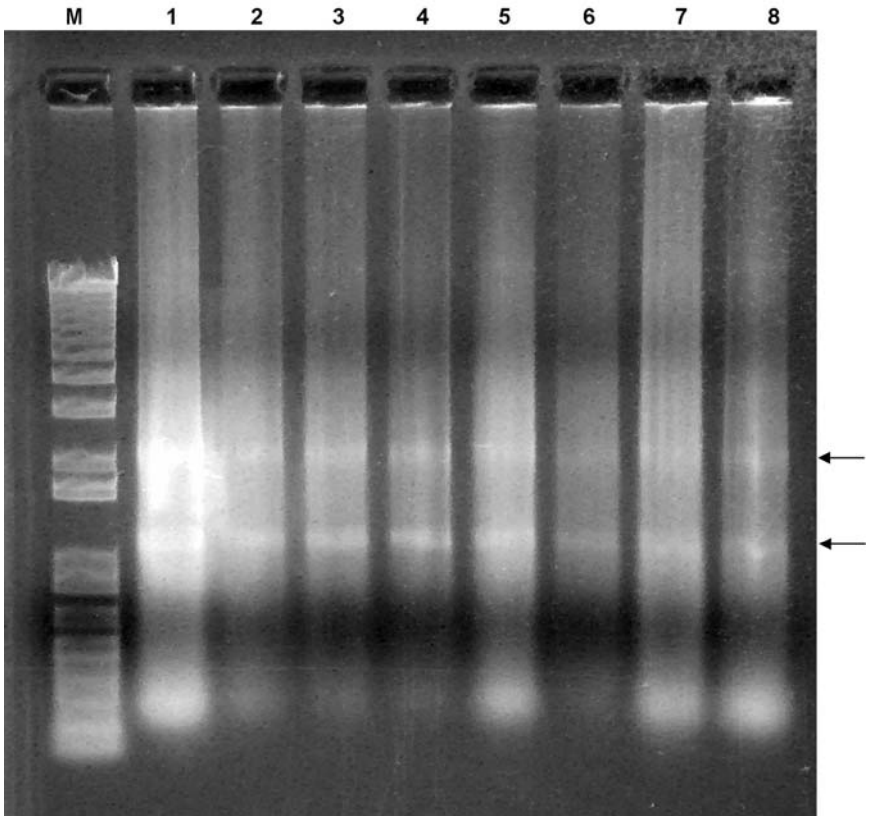

Figure 4.1. Purified total RNA visualized on a 1.0% agarose gel. Lane M: 1 Kb Plus DNA Ladder. Lanes 1 – 8: One µl of puried total RNA from eight different samples. Bands are apparent for the abundant 28S and 18S ribosomal RNA around 4.5 kb and 1.9 kb, respectively (arrows).

4.2 Suppression Subtractive Hybridization

Messenger RNA was isolated from total RNA and subjected to SSH to construct a subtracted cDNA library enriched in transcripts that were preferentially expressed in PND 0 than PND 28 and on PND 28 than in PND 56.

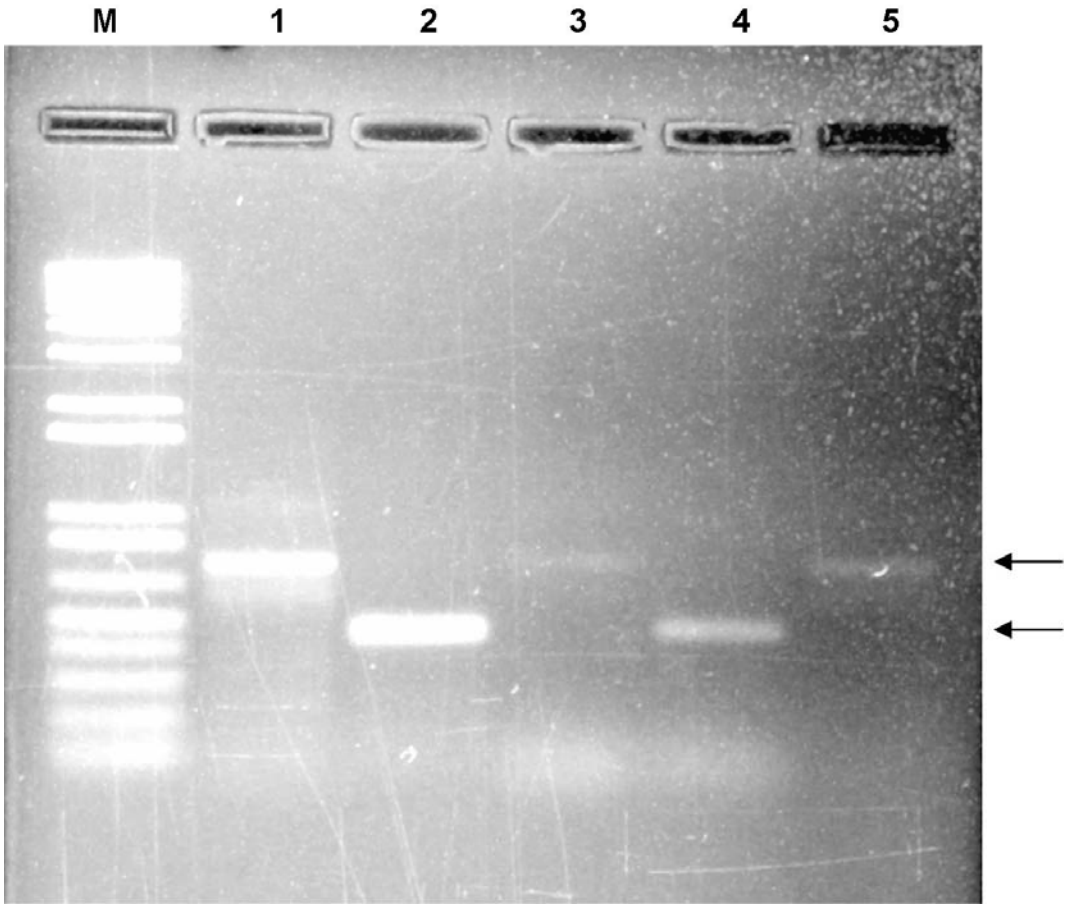

Figure 4.2. Efficiency of adaptor ligation of control reaction visulaized on agarose gel. Lane M) 1 kb plus DNA ladder. Lane 1) PCR products with Tester 1-1 (Adaptor 1 ligated) as the template and G3PDH 3' Primer and PCR Primer 1. Lane 2) PCR products with Tester 1-1 (Adaptor 1 ligated) as the template and G3PDH 3' and 5' Primers. Lane 3) PCR products with Tester 1-2 (Adaptor 2R ligated) as the template and G3PDH 3' Primer and PCR Primer 1. Lane 4) PCR products with Tester 1-2 (Adaptor 2R ligated) as the template and G3PDH 3' and 5' Primers. Lane 5) More dilute Tester 1-1 with PCR Primer 1. Efficiency was determined by a shift in molecular weight (MW) when G3PDH was amplified in control cDNA using the PCR Primers (1 and 2R) (top arrow) versus gene specific primers (G3PDH) 3' and 5' (bottom arrow).

Tester and driver cDNA were generated then blunt-ended by *Rsa* I digestion. One of two adaptors were ligated to the cDNA and efficiency was determined based on whether there was a detectible shift in molecular weight (MW) between second-strand synthesis products and *Rsa* I digested products of the control reaction (Figure 4.2). Subtracted products were successfully amplified as determined visually on a 1/5% agarose gel (Figure 4.3). Abundance of products were low following primary amplification, but distinct bands were apparent after secondary PCR.

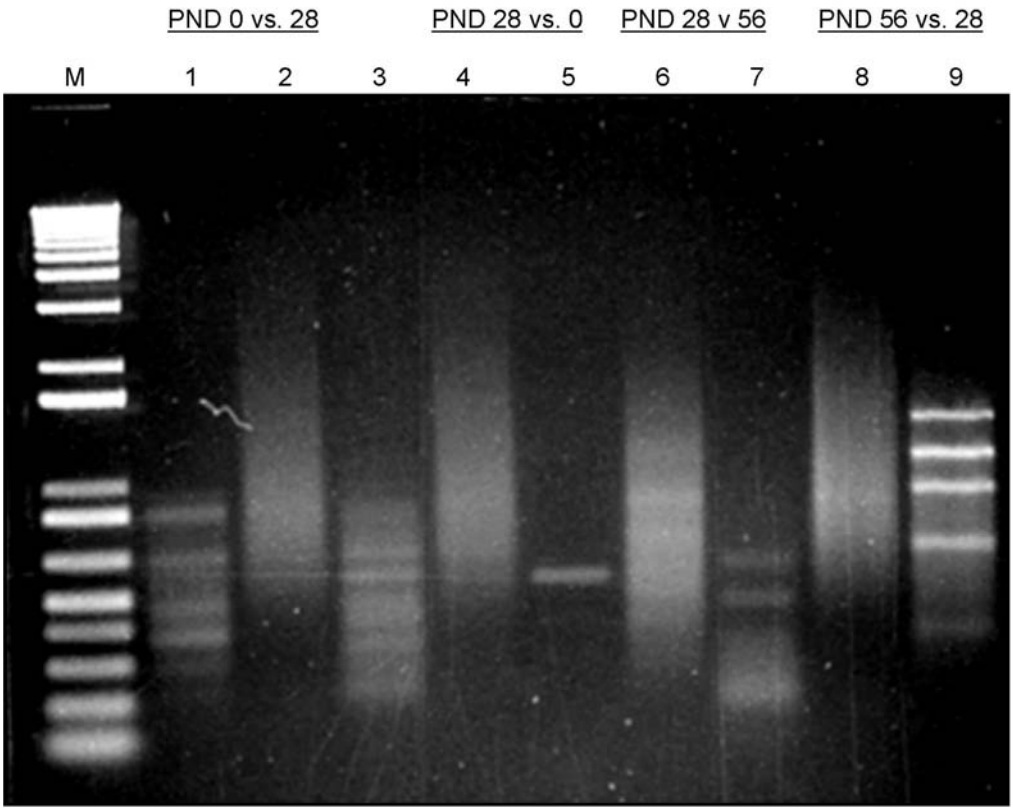

Figure 4.3. Secondary PCR of subtracted and unsubtracted products visualized on agarose gel. Subtracted tester and driver cDNA show individual bands, whereas unsubtracted tester and driver cDNA show streaks. Lane: M) 1 kb Plus DNA ladder, 1) PND 0 Tester Subtracted cDNA. 2) PND 0 Tester Unsubtracted cDNA ligated with both Adaptors 1 and 2R. 3) PND 28 Tester (PND 0 Driver) Subtracted cDNA. 4) PND 28 Tester (PND 0 Driver) Unubtracted cDNA ligated with both Adaptors 1 and 2R. 5) PND 28 Tester (PND 56 Driver) Subtracted cDNA. 6) PND 28 Tester (PND 56 Driver) Unsubtracted cDNA ligated with both Adaptors 1 and 2R. 7) PND 56 Tester Subtracted cDNA. 8) PND 56 Unsubtracted cDNA ligated with both Adaptors 1 and 2R. 9) PCR Control Subtracted cDNA.

4.3 Differential Screening, DNA Sequencing, and *Eco*R I Digestion

Electronic images of membranes were used to determine differential expression based on the criteria in Table 4.1. In addition to differential screening, all clones were *Eco*R I digested to determine approximate insert size (MW). Plasmids showed either no insert or different molecular weight bands, indicating the presence of multiple inserts (Figure 4.4). A total of 288 SSH products were screened in two forward and reverse experiments. Of these, 67 were identified to be differentially expressed through dot-blot hybridization assays using DIG-labeled probes (Figures 4.5-4.8). Only 34 were subjected to sequencing and BLAST analysis.

Table 4.1. Interpretation of hybridization assay screening from differential expression.

Probes				Analysis
1. Forward Subtracted	**2. Forward Unsubtracted**	**3. Reverse Subtracted**	**4. Reverse Unsubtracted**	
+	+	-	-	Differentially expressed products
+	-	-	-	Low abundance products
+ > 5	+	+	-	Differentially expressed products
+	+	-	+	Significantly different from reverse subtracted
+, -	+, -	+, -	+, -	No differential expression

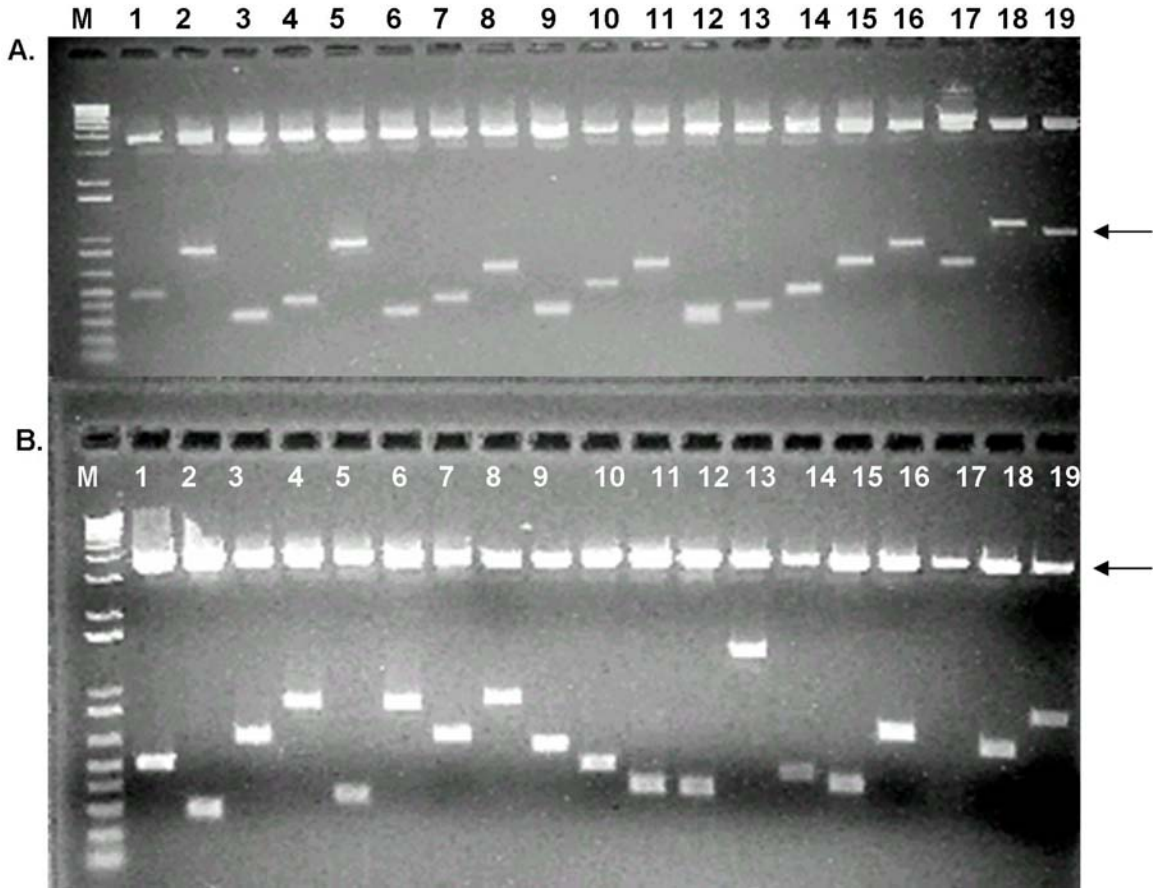

Figure 4.4. *EcoR* I digested clone products. Lane M: 1 Kb Plus DNA ladder. Remaining Lanes (1-19): individual clones digested with *Eco*R I show distinct bands (A. arrow) at MW lower than plasmid DNA (B. arrow). Clones with no insert show no distinct band, such as in Panel B, Lane 17.

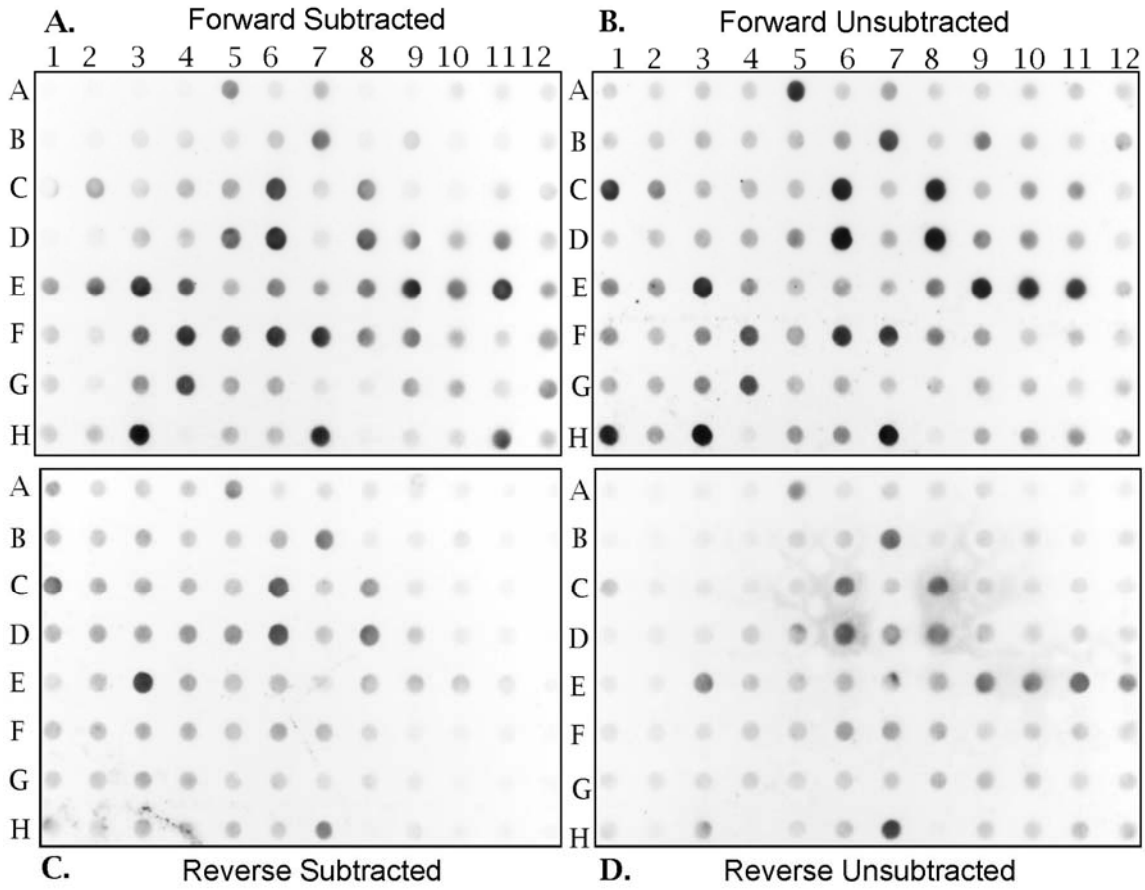

Figure 4.5. Differential screening analysis of PND 0 versus PND 28 hybridization assays using DIG-labeled probes. Differentially screened nylon membranes spotted with purified plasmid DNAs from subtracted population when PND 0 was the tester and PND 28 was the driver. Membranes were probed with A) tester subtracted from driver (forward subtracted), B) tester unsubtracted with both adaptors present but no driver present, C) PND 28 as tester and PND 0 as driver (reverse subtracted), D) reverse unsubtracted (absence of PND 0, driver added and both adaptors present). DIG-labeled probes (25 ng/ml) hybridized (42°C overnight), detected through CSPD, and exposed to X-OMAT blue film for approximately 30 sec.

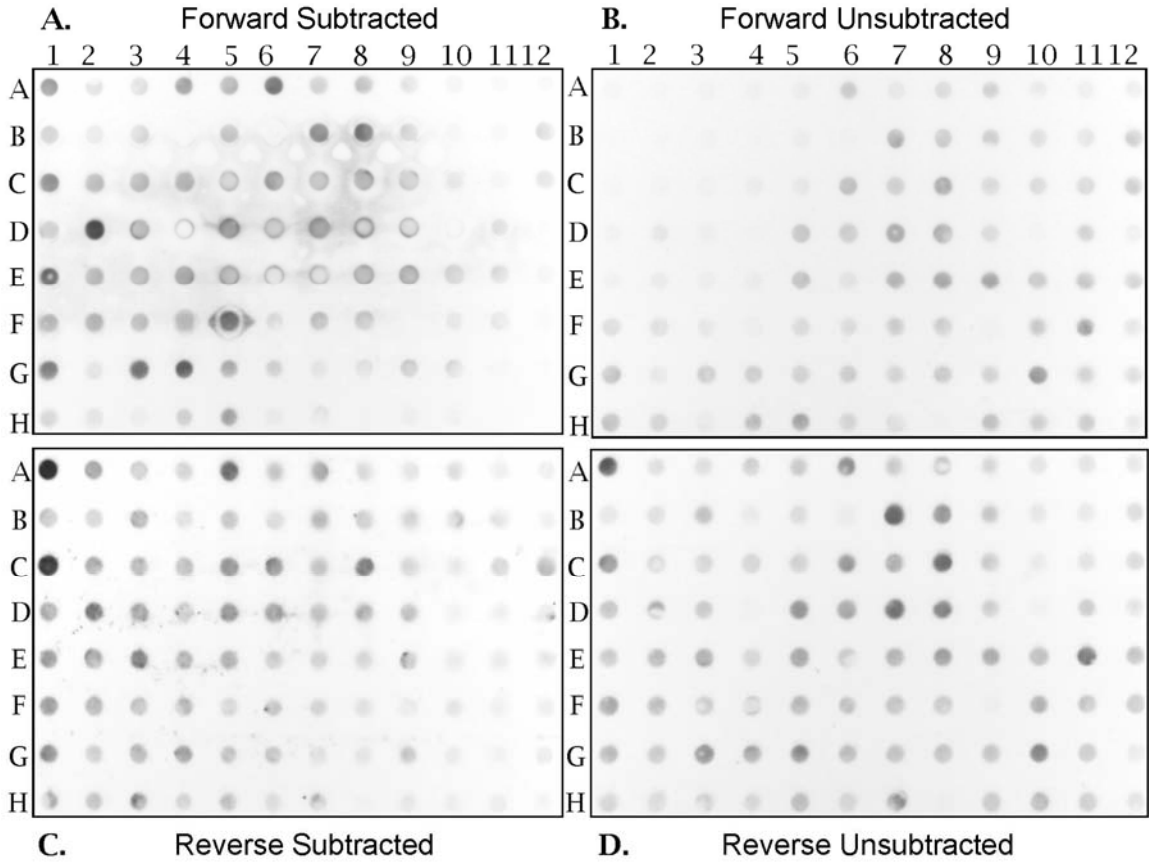

Figure 4.6. Differential screening analysis of PND 28 versus PND 0 hybridization assays using DIG-labeled probes. Differentially screened nylon membranes spotted with purified plasmid DNAs from subtracted population when PND 28 was the tester and PND 0 was the driver. Membranes were probed with A) tester subtracted from driver (forward subtracted), B) tester unsubtracted with both adaptors present but no driver present, C) PND 0 as tester and PND 28 as driver (reverse subtracted), D) reverse unsubtracted (absence of PND 28, driver added and both adaptors present). DIG-labeled probes (25 ng/ml) hybridized (42°C overnight), detected through CSPD, and exposed to X-OMAT blue film for approximately 30 sec.

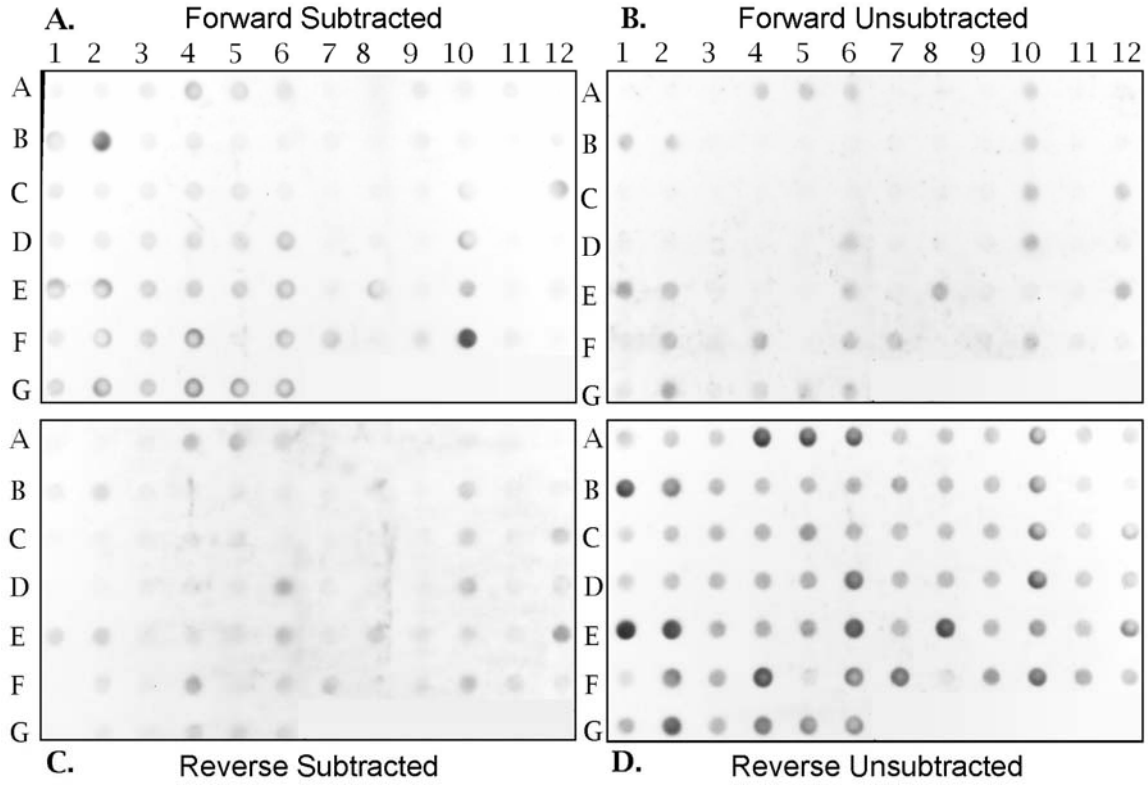

Figure 4.7. Differential screening analysis PND 28 versus PND 56 hybridization assays using DIG-labeled probes. Differentially screened nylon membranes spotted with purified plasmid DNAs from subtracted population when PND 28 was the tester and PND 56 was the driver (Clones 1-76). Membranes were probed with A) tester subtracted from driver (forward subtracted), B) tester unsubtracted with both adaptors present but no driver present, C) PND 56 as tester and PND 28 as driver (reverse subtracted), D) reverse unsubtracted (absence of PND 28, driver added and both adaptors present). DIG-labeled probes (25 ng/ml) hybridized (42°C overnight), detected through CSPD, and exposed to X-OMAT blue film for approximately 45 sec.

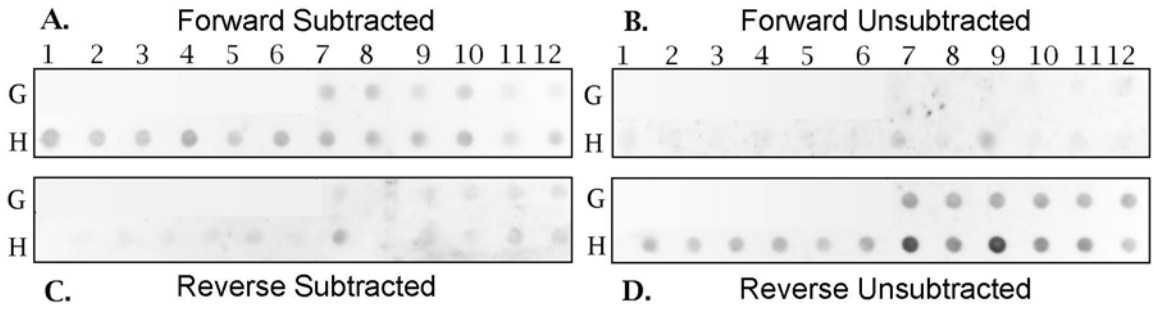

Figure 4.8. Differential screening analysis PND 56 versus PND 28 hybridization assays Using DIG-labeled Probes. Differentially screened nylon membranes spotted with purified plasmid DNAs from subtracted population when PND 56 was the tester and PND 28 was the driver (Clones 1-18). Membranes were probed with A) tester subtracted from driver (forward subtracted), B) tester unsubtracted with both adaptors present but no driver present, C) PND 28 as tester and PND 56 as driver (reverse subtracted), D) reverse unsubtracted (absence of PND 0, driver added and both adaptors present). DIG-labeled probes (25 ng/ml) hybridized (42°C overnight), detected through CSPD, and exposed to X-OMAT blue film for approximately 45 sec.

Sequence analysis revealed 25/34 quality readings and 16/25 matched known sequences, while 7/25 returned identity to uncharacterized clones, and 2/25 had no significant match to any known sequences. Differential screening results are summarized in Table 4.2. Sequence identity for each subtraction are summarized in Tables 4.3 and Table 4.4. Two clones from the PND 0 vs. PND 28 forward subtraction and one from the reverse subtraction were chosen to perform qRT-PCR analysis. For the forward subtraction, clones PND 0 vs. PND 28 #45 (SPARCL1) (Figure 4.5, Panels A-D, Lane D, Column 9) and #47 (Figure 4.5, Panels A-D, Lane D, Column 11) were selected because each showed labeling on both the forward subtracted and unsubtracted membranes, but with lower expression in the reverse subtracted and unsubtracted membranes. Clone PND 28 vs. PND 0 #7 (Figure 4.6, Panels A-D, Lane A, Column 7) was chosen as a control since labeling appeared similar on each subtracted membrane.

Table 4.2. Summary of differential screening and sequencing of subtracted clone libraries.

Subtraction	Expression	No. Clones	No. Diff.	No. Seq.	No. Good	No. Known	No. Unk.
PND 0 vs. PND 28	> in 0	96	35	17	14	10	4
PND 28 vs. PND 0	> in 28	96	19	13	10	6	4
PND 28 vs. PND 56	> in 28	78	13	2	1	0	1

Table 4.3. PND 0 vs. PND 28 clone sequence results.

Clone	ACC. #	Name	% Match
PND0v28_5	CN153472	EF1ALPHA	764/776 (98%)
PND0v28_7	AF304203	Mitochondrion, partial genome	290/300 (96%)
PND0v28_30	CK463699	EF1ALPHA	344/350 (98%)
PND0v28_45	BQ604418	Pig uterine clone: similar to human SPARCL1	580/583 (99%)
PND0v28_47	BP169911	Pig uterine clone: transcribed sequences	538/541 (99%)
PND0v28_49	CF367529	Pig uterine clone	163/176 (92%)
PND0v28_50	AF304203	Mitochondrion, partial genome	205/209 (98%)
PND0v28_59	BP438017	EF1ALPHA	621/625 (99%)
PND0v28_70	AB113356.1	Pig clone	345/379 (91%)
PND0v28_72	BP441417	Pig clone: similarity to human POLR2C	310/310 (100%)
PND0v28_76	AF304203	Mitochondrion, partial genome	136/144 (94%)
PND0v28_84	CK456781	Pig clone: similarity to human PABPC1	679/680 (99%)
PND0v28_95	BP169911	Pig uterine clone: transcribed sequences	513/517 (99%),

Table 4.4. PND 28 vs. PND 0 clone sequence results.

CLONE	ACC. #	Name	% Match
PND28v0_6	CB169367	Bos taurus clone	309/371 (83%)
PND28v0_7	CK458228	Pig embryo clone: transcribed sequences	395/397 (99%)
PND28v0_8	AJ685413	Pig clone: COL3A1	456/490 (93%)
PND28v0_19	AC104479.3	Pig clone	236/259 (91%)
PND28v0_20	BP463666	Pig uterus clone: similarity to human 40S	468/491 (95%)
PND28v0_24	AJ604634	Pig clone: similarity to human 40s	308/317 (97%)
PND28v0_56	AJ663726	Pig clone: similarity to human COL1A2	188/195 (96%)
PND28v0_81	AJ682260	POLR2B	328/331 (99%)
PND28v0_82	BP463666	Pig uterus clone: similarity to human 40S	492/501 (98%)

4.4 Quantitative Real-Time PCR

Gene expression profiles during postnatal uterine development were generated for three clones chosen for analysis based on differential expression as determined by DIG-labeling. The function of two clones (PND 0 vs. PND 28 #47 and PND 28 vs. PDN0 #7) are currently unknown, while SPARCL1 has been indicated in determination of cellular adhesion [Nomura *et al.*, 1988]. Abundance of these genes were determined using qRT-PCR.

Primers were designed (Table 4.5) and concentrations were optimized (Figure 4.9) so that a 10-fold dilution resulted in a difference of 3 cycle thresholds. A melting curve analysis (dissociation curve) was performed for transcripts (Figure 4.10) to determine the optimal temperature for fluorescent data acquisition. As seen in the figure, nonspecific amplification, including primer-dimers, was indicated by the initial fluorescent peak with a characteristic lower T_M. In this example, the specific products were shown with a T_M around 92^{o}C and nonspecific products with a T_M around 86^{o}C.

The optimal temperature to acquire fluorescence data was after nonspecific dissociation and before product dissociation. In Figure 4.10, the optimal data acquisition was around 88^{O}C. Data acquisition for the targets was 76^{O}C for PND 0 vs. PND 28 #45 and #47 and 72^{O}C for PND 28 vs. PND 0 #7 (Table 4.5)

Table 4.5. Quantitative RT-PCR primer list for targets SPARCL1, Clone PND 0 vs. PND 28 #47, and clone PND 28 vs. PND 0 #7.

Target	Sequence	Data Acquistion (^{O}C)
SPARCL1	Forward 5'-TCC TTC AGG GTG ATG TGC TTA TCC-3' Reverse 5'-GCA GTT CAG TGA GCT TGA CCA ACA-3'	76
PND0_47	Forward 5'-TCA TTC ACC CTC ATC GTG TCT CCA-3' Reverse 5'-AAG AAA CCA CCT CCC ACC TGC TTA-3'	76
PND28_7	Forward 5'-GGG TTG CCA TCA CAA ATC ATC GCT A-3' Reverse 5'-CCC AGA CAC ATC CAT GTT CAT GCA AAC-3'	72

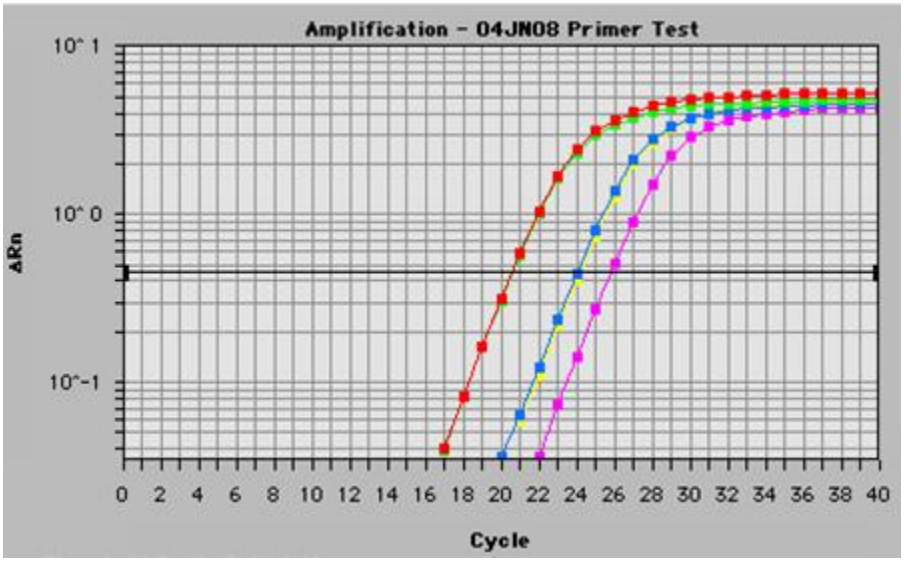

Figure 4.9. Sample amplification plot from primer optimization for SYBR green assay. Wells B1 and B2: 50 ng total RNA. Wells B3 and B4: 5 ng total RNA. Well B5: No Template Control (NTC).

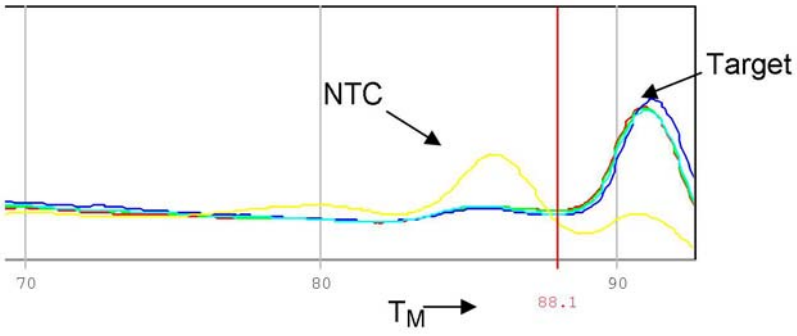

Figure 4.10. Melting curve analysis of primers for qRT-PCR. This melting curve analysis indicates that primer-dimers form in the no template control (NTC) samples and had an approximate T_M of 86°C, as indicated by the single yellow peak. Reactions with template amplify target cDNA, resulting in a higher T_M around 92°C. Target amplicons are indicated by the green, blue, and red peaks, which were shifted to the right of the NTC. Appropriate data acquisition was at the temperature greater the NTC primer-dimer T_M, yet less than the T_M of the amplicon. This ensured that fluorescence was acquired only from the double-stranded target.

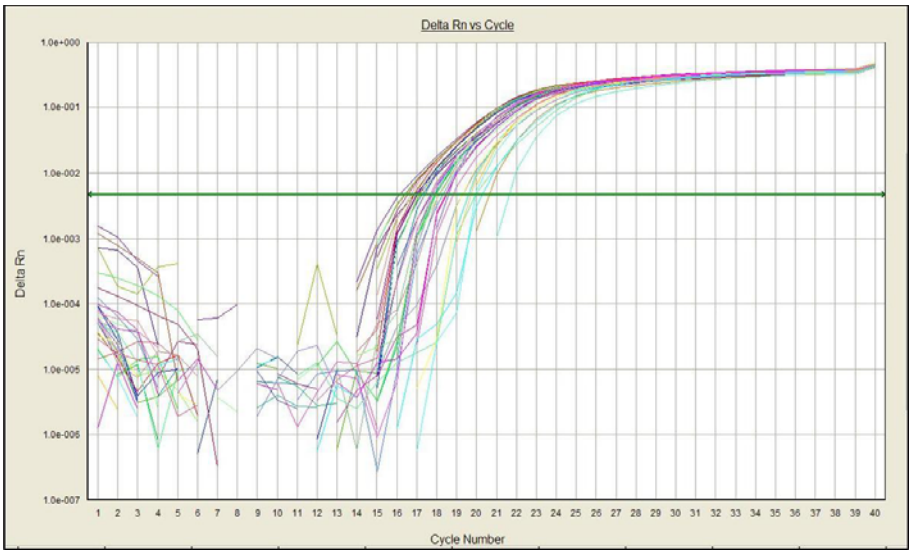

Figure 4.11. Amplification plot of SPARCL1 (PND 0 vs. PND 28 #45) qRT-PCR using SYBR green. Note that the threshold was set at the geometric phase of the curve.

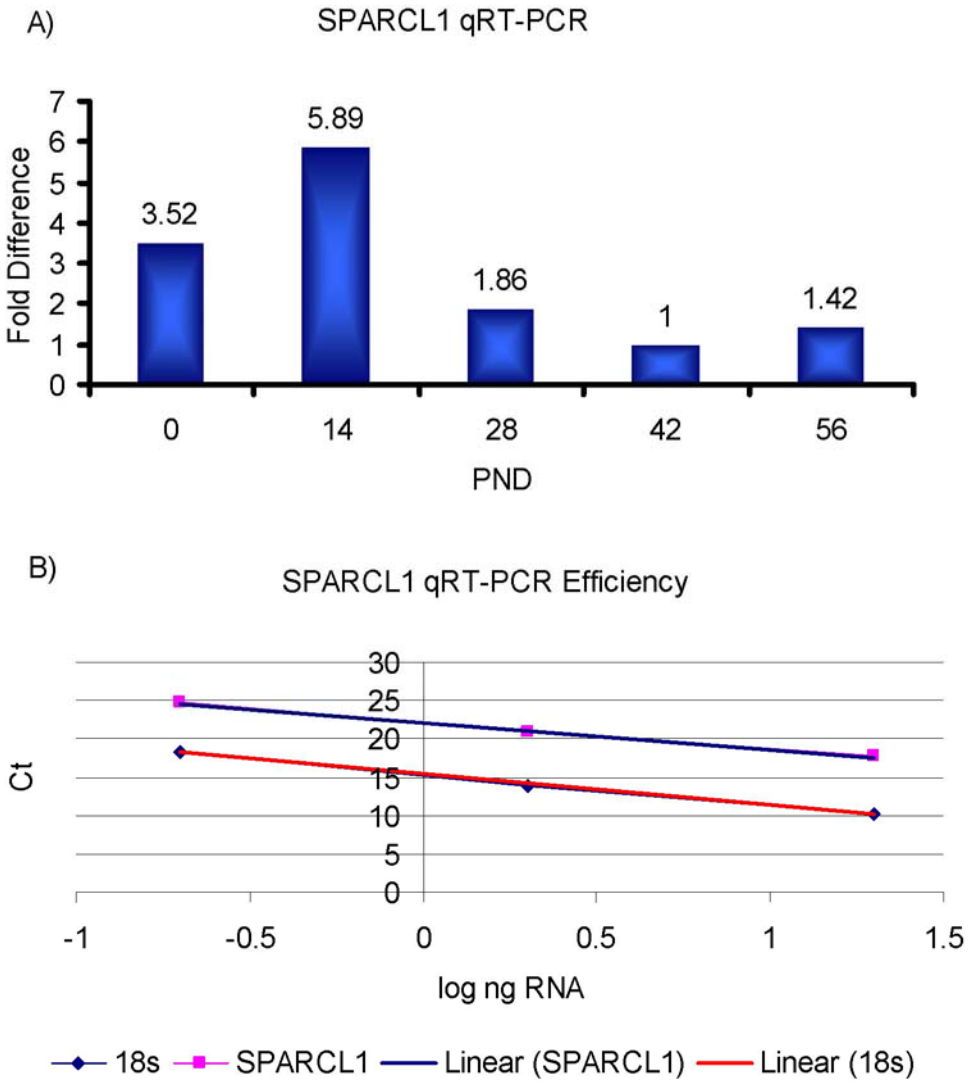

Figure 4.12. Quantitative RT-PCR of SPARCL1 (PND 0 vs. PND 28 #45) transcripts in postnatal uterine tissue. Panel A) Fold difference in mRNA expression of SPARCL1 in postnatal pig uteri. There was a significant increase in expression by PND 14, with significant decrease by PND 28 through 56 ($P \leq 0.05$), indicating a possible role of SPARCL1 during the proliferative stage of development. Panel B) Efficiency of qRT-PCR based on the difference in slope of target (-3.565) and 18S (-4.0325) expression in 20, 2, and 0.2 ng total RNA. Difference in slopes was 0.4675.

Fold differences in transcript abundance were based on normalization with 18S ribosomal RNA (Table 4.6). Expression of SPARCL1 mRNA significantly increased ($P \leq 0.05$) in expression at PND 0 and 14, with significant decrease by PND 28 through 56. The amplification plot (Figure 4.11) was evaluated to determine linear amplification of target gene as indicated by a sigmoidal curve. Fold changes were determined by the $2^{-\Delta\Delta Ct}$ method (Figure 4.12a). Postnatal Day 42 was set as the normalizer since it had the least abundant transcripts. When compared to PND 42, PND 0 had 3.5-fold greater SPARCL1 transcripts, then expression increased at PND 14 to 5.89-fold, followed with a rapid decline in expression by PND 28 that continued until PND 56.

Clone PND 0 vs. PND 28 #47 (accession BP169911) quantitation was not significantly different ($P \leq 1.0$) during development. Amplification of transcripts was determined by the amplification plot (Figures 4.13) and fold differences calculated (Figure 4.14a). The normalizer was PND 28 as it had the least abundant transcripts and expression started at moderate levels, then increased to 2.3-fold at PND 14, before declining again at PND 28. There was slight difference in gene expression between PND 0 and 28 as determined by differential screening.

Transcripts for clone PND 28 vs. PND 0 #7 (accession CK458228) were low at birth (PND 0), significantly increased ($P \leq 0.05$) by PND 14, then declined to initial levels. Fold differences were determined by setting PND 42 as the normalizer. When compared to the normalizer, expression of the clone was similar at PND 0, then increased 2.22-fold at PND 14, before slowly declining to normalized expression at PND 28 (Figure 4.15a).

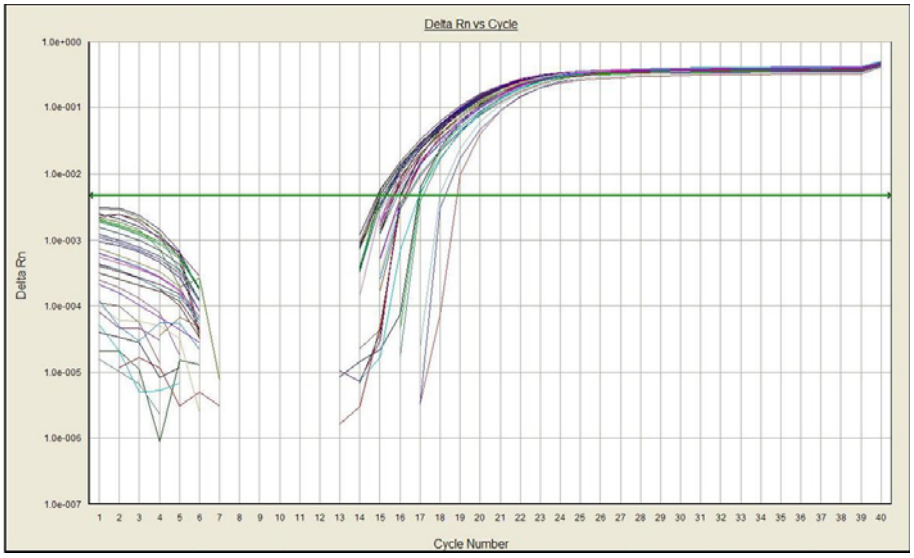

Figure 4.13. Amplifcation plot of PND 0 vs. PND 28 #47 qRT-PCR using SYBR green. Note that the threshold was set at the geometric phase of the curve.

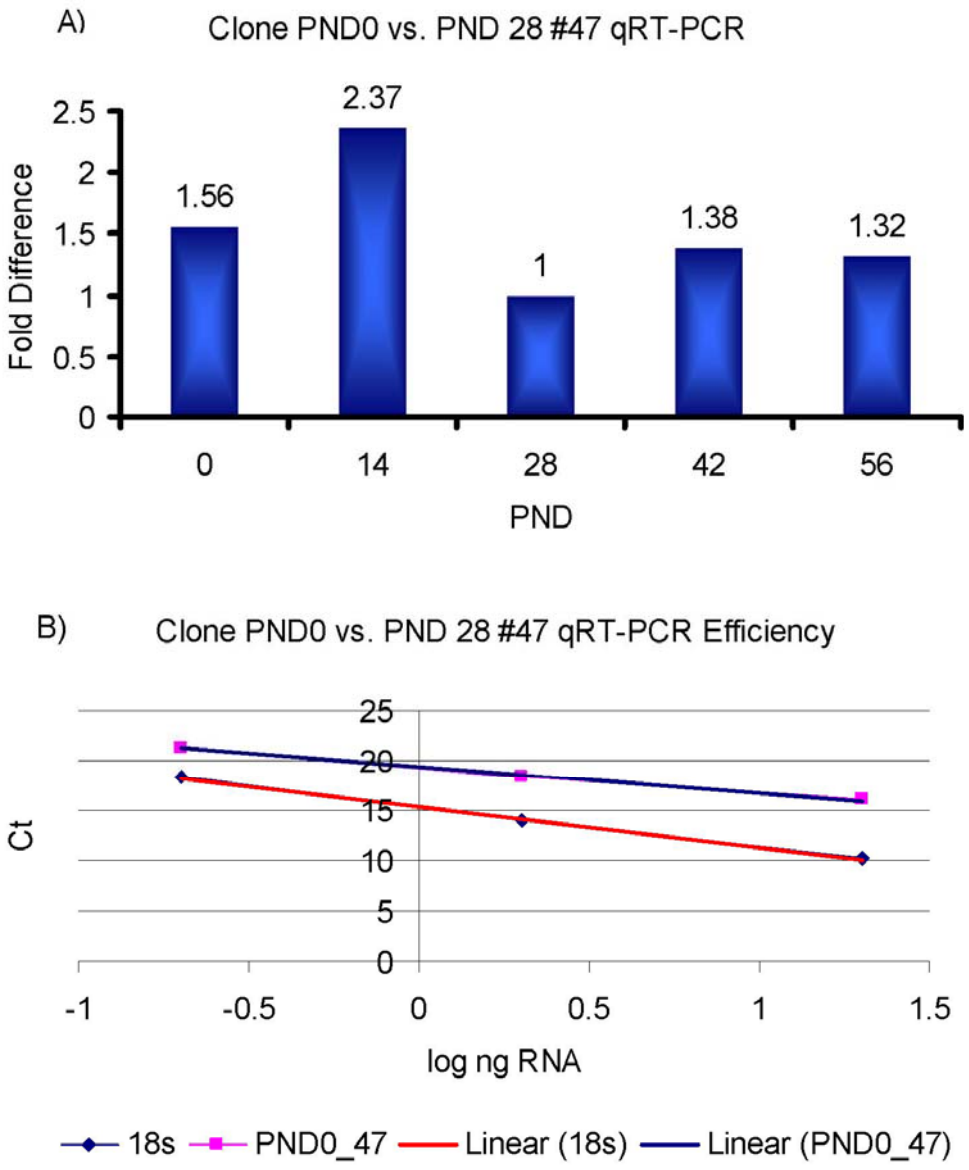

Figure 4.14. Quantitative RT-PCR of clone PND 0 vs. PND 28 #47 transcripts in postnatal uterine tissue. Panel A) Fold difference in mRNA expression of clone PND 0 vs. PND 28 #47 (accession BP169911) in postnatal pig uteri. There was no significant difference in mRNA expression during development, but there was a slight increase at PND 14. Panel B) Efficiency of qRT-PCR based on the difference in slope of target (-2.63) and 18S (-4.0325) expression in 20, 2, and 0.2 ng total RNA. Difference in slopes was 1.403.

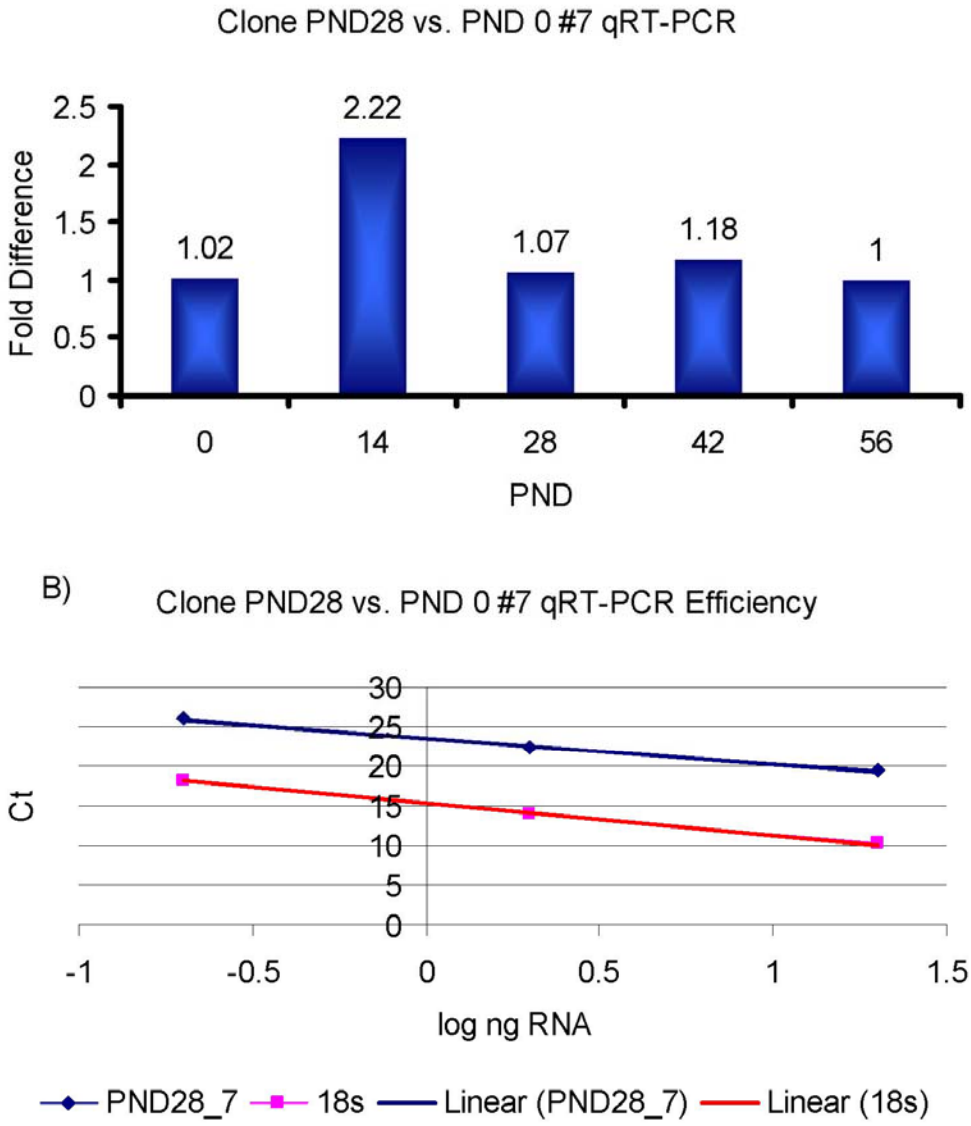

Figure 4.15. Quantitative RT-PCR of clone PND 28 vs. PND 0 #7 transcripts in postnatal uterine tissue. Panel A) Fold difference in mRNA expression of clone PND 28 vs. PND 0 #7 (accession CK458228) in postnatal pig uteri. Expression was low at birth (PND 0), significantly increases by PND 14 to 2-fold, then declines to initial levels. The role of this clone us presently unknown, nevertheless it was more active during the proliferative stage of development. Panel B) Efficiency of qRT-PCR based on the difference in slope of target (-3.2838) and 18S (-4.0325) expression in 20, 2, and 0.2 ng total RNA. Difference in slopes was 0.7847.

Table 4.6. Quantitative RT-PCR analysis of gene expression for SPARCL1, clone PND 0 vs. PND 28 #47, and clone PND 28 vs. PND 0 #7 in neonatal pig uteri during early postnatal growth.

		Target	18S			
Target	**PND**	**Average C_T***	**Average C_T***	**ΔC_T†**	**$\Delta\Delta C_T$‡**	**$2^{-\Delta\Delta CT}$ §**
SPARCL1	0	17.27 ± 0.45	10.32 ± 0.09	6.94 ± 0.25 ^{bc}	1.817	3.5247
	14	16.65 ± 0.42	10.45 ± 0.29	6.20 ± 0.09 ^{c}	2.56	5.8971
	28	18.12 ± 1.17	10.26 ± 0.06	7.86 ± 0.79 ^{ab}	0.902	1.8693
	42	19.39 ± 1.01	10.63 ± 0.25	8.76 ± 0.54 ^{a}	0	1
	56	18.67 ± 1.00	10.42 ± 0.32	8.25 ± 0.48 ^{a}	0.511	1.4253
PND0	0	15.67 ± 0.68	10.32 ± 0.09	5.35 ± 0.42	0.645	1.5637
#47	14	15.19 ± 0.42	10.45 ± 0.29	4.75 ± 0.09	1.25	2.3784
	28	16.25 ± 1.43	10.26 ± 0.06	5.99 ± 0.97	0	1
	42	16.15 ± 0.90	10.63 ± 0.25	5.53 ± 0.45	0.471	1.3863
	56	16.01 ± 0.54	10.42 ± 0.32	5.59 ± 0.15	0.403	1.3222
PND28	0	20.04 ± 0.45	10.32 ± 0.09	9.72 ± 0.25 ^{a}	0.033	1.0232
#7	14	19.05 ± 0.25	10.45 ± 0.29	8.60 ± 0.03 ^{b}	1.155	2.2268
	28	19.90 ± 0.53	10.26 ± 0.06	9.64 ± 0.33 ^{a}	0.110	1.0796
	42	20.13 ± 0.46	10.63 ± 0.25	9.50 ± 0.14 ^{a}	0.250	1.1897
	56	20.17 ± 0.90	10.42 ± 0.32	9.75 ± 0.41 ^{a}	0	1

* Cycle Threshold (C_T) reflects the cycle number that target or 18S amplicon fluorescence crossed the geometric phase of the amplification curve.

† Normalized CT Values (ΔC_T) indicates the mean target transcript C_T less the 18S C_T. Allows for the normalization of target C_T in relation to endogenous 18S ribosomal RNA CT.

‡ Calibrated Value ($\Delta\Delta C_T$). The PND value in which had the greatest ΔC_T (or least abundant transcript) for each target was set as the calibrator. Normalized ΔC_T values were subtracted from the calibrator.

§ Fold Difference ($2^{-\Delta\Delta Ct}$) was determined by each calibrated value.

$^{a-c}$ Values with different superscript letters indicate a significant difference ($P \leq 0.05$) between samples, while values with same superscript letters indicate no significant difference. Statisical analysis was carried out using least squared means (LSM) from PROC MIXED of Statistical Analysis Systems (SAS).

Chapter 5: DISCUSSION

The onset of uterine gland morphogenesis is a postnatal event in pigs [Hadek and Getty, 1959; Bal and Getty, 1970; Spencer *et al.*, 1993a], sheep [Wiley *et al.*, 1986; Bartol *et al.*, 1988a; 1988b], and rodents [Branham *et al.*, 1985]. In pigs, the time from birth until PND 14 involves a general increase in uterine size, as evident by increased uterine weight and thickness [Hadek and Getty, 1959; Tarleton *et al.*, 1999].

Existing research clearly indicates the necessity for uterine glands to sustain normal uterine function. These highly branched and coiled glands synthesize and secrete or transport substances collectively known as histotroph. Proteins of histotroph provide pre-attachment nourishment and growth factors critical to conceptus survival. Animals in which uterine gland function is postnatally inhibited, such as the ovine UGKO and porcine estrogen-induced uterine disruption, the ability of the adult uterus to maintain normal pregnancy is compromised. The significance of glands for uterine function is known; however, the mechanisms that regulate uterine morphogenesis, proliferation, and function are not as well understood.

Characterization of specific gene expression during postnatal uterine adenogenesis in the pig offers beneficial information concerning significant developmental processes critical to peri-implantation conceptus survival. This knowledge may serve as the basis to enhance reproductive development and uterine function by positively influencing conceptus survival and development.

The use of suppression subtractive hybridization (SSH), which is based on

suppression PCR [Diatchenko *et al.*, 1996], allowed for comparison of gene expression profiles between various stages of development. With SSH, target cDNA fragments (differentially expressed) are selectively amplified while nontarget cDNA amplification is suppressed. Advantages to this technique include the ability to begin SSH with small amounts of starting material (2 µg poly A^+ RNA). Both high and low abundance sequences are equalized during normalization and the method can be complete in just a few days. There are also disadvantages to SSH. First, the average cDNA size is small (0.1 to 2 kb) due to blunt-ended *Rsa* I restriction enzyme digestion. However, the cDNA sizes are adequate for BLAST analysis. Furthermore, differential screening steps are necessary to minimize the background and eliminate possible false-positives. The present work utilized SSH to create unique cDNA libraries respective to postnatal development at 3 stages: Day 0 when only shallow depressions can be observed, Day 28 when branching morphogenesis begins, and Day 56 when glands are well established.

When PND 0 was compared with PND 28, many genes identified in the forward subtraction, those greater at Day 0 versus Day 28, encode products involved in transcription or translation, including elongation factor 1 alpha 1 (EF1a1), poly(A) binding protein, cytoplasmic 1 (PABPC1), and polymerase (RNA) II (DNA directed) polypeptide C (POLR2C / RPB3).

In addition to its role during translation, EF1a1 has been suggested to be involved with inhibition of apoptosis [Talapatra *et al.*, 2002] and shows high tumor-specific expression, relative to normal tissue [Lee, 2003]. Poly(A) binding protein, cytoplasmic 1 (PABPC1) is involved in the initiation of translation and mRNA turnover [Kozlov *et al.*, 2001]. It is found in both the cytosol and nucleus [Grange *et al.*, 1987] of eukaryotes and associated with the poly(A) tail of newly synthesized mRNA [Schwartz

and Darnell, 1976]. It acts as a scaffolding protein and recruits additional translation factors for mRNA translation [Kozlov *et al.*, 2001]. The RNA polymerase polypeptide POLR2C, also known as RPB3, is most commonly known regarding its structural function in the polymerase II subassembly and is involved in the transcription of protein coding genes [Song *et al.*, 1994].

The other gene of interest was secreted protein, acidic, cysteine-rich-like 1 (SPARCL1), which influences several cellular activities and is a member of the SPARC protein family. SPARC proteins are classified as matricellular proteins that function to bind to matrix proteins, cell surface receptors, cytokines, and proteases that interact with cells to regulate cell shape via “anti-adhesive” effects which ultimately leads to cell rounding and partial detachment from a substratum [Sage and Bornstein, 1991]. SPARC has been referred to as 1) osteonectin, a major non-collagenous constituent of human and bovine bone [Termine *et al*., 1981], 2) a BM40, a component of the basement membrane [Dziadek *et al*., 1986], and 3) SPARC (Secreted Protein Acidic and Rich in Cysteine) from mouse parietal endoderm [Mason *et al*., 1986]. The anti-adhesive cell-matrix regulator glycoprotein SPARC [Johnston *et al*., 1990; Lane and Sage, 1994] has been shown to inhibit cell spreading on collagen and induce cell rounding in cultured endothelial cells and fibroblasts [Sage *et al*., 1989]. Such changes in cell adhesion mediated by SPARC are thought to influence a number of cellular activities including proliferation, migration, and differentiation [Bradshaw and Sage, 2001].

The SPARC protein family has a similar basic structure of acidic residue clusters, a follistatin-like cysteine-rich region, and a high affinity calcium binding region, termed an EF hand [for review see Lane and Sage, 1994]. This protein family is extracellular and mediates cell-matrix interactions [Sage and Bornstein, 1991]. The SPARC protein has domains that can function independently to bind cells and matrix components [Engel *et*

al., 1987]. Domain I is highly acidic and has a relatively low binding affinity for calcium [Lane and Sage, 1994]. Domain II is homologous to a repeated domain in follistatin, a cytokine inhibitor. Domains II an IV (termed the extracellular [EC] domain) bind calcium to collagen IV [Maurer *et al*., 1995]. The member SPARCL1 has been referred to as 1) SC1 in mice [Johnston *et al*., 1990], 2) hevin from human tonsil high endothelial venule cells [Girard and Springer, 1996], 3) mast9 (magnet-assisted subtraction technique) in lung carcinoma [Schraml *et al*., 1994], and 4) renamed to SPARC-like 1 (SPARCL1) due to its high homology to SPARC-protein family members [Isler *et al*., 2001]. SPARCL1 has approximately 65% conservation with the last two-thirds of SPARC [Girard and Springer, 1996]. Due to the homology between SPARCL1 and SPARC, it is possible that SPARCL1 shares some of the same features.

In addition to regulating cell shape, SPARC regulates the activity of several growth factors including TGF-β1 [Francki *et al*., 1999] and binds to ECM proteins such as collagen type I [Sasaki *et al*., 1998] via the extracellular calcium-binding domain [Maurer *et al*., 1997]. A study in mice indicated that SPARC stimulates collagen type I production through a TGF-β1-dependent pathway [Francki *et al*., 1999]. In many tissues, the ECM is composed of collagens, proteoglycans, and non-collagenous glycoproteins that form complex structures. SPARCL1 involvement in cell-matrix interactions is supported by the expression of hevin from human high endothelial venule (HEV) cells [Girard and Springer, 1996]. Girard and Springer [1996] showed that SPARCL1 (hevin) was associated with the basal, lateral, and apical surfaces of HEV cells and is not expressed in the underlying basement membrane. Furthermore, purified SPARCL1 did not support human umbilical vein endothelial cell adhesion *in vitro* and exogenous SPARCL1 inhibited attachment and spreading of endothelial cells on fibronectin substrates [Girard and Springer, 1996], while inhibition of cell spreading is concentration dependant [Lane and Sage, 1990].

The expression of SPARCL1 is variable. It is expressed in rat embryonic and adult neurons in the central nervous system with the highest levels in the adult brain [Johnston *et al*., 1990]. Soderling and coworkers [1997] detected SPARCL1 in adult mouse lung bronchi and bronchioles, larger vessels of cardiac muscle, vessels in the liver, and throughout the red pulp of the spleen. SPARCL1 was not detected in cultured and proliferataing endothelial cells or smooth muscle cells [Soderling *et al*., 1997]. Isler and coworkers [2001] proposed that SPARCL1 may function to mediate cell matrix interactions to support cellular differentiation, and not promoting proliferation. Claeskens and coworkers [2000] showed in HeLa3S cancer cells that overexpression of SPARCL1 reduced cell proliferation. SPARCL1 has been shown to be down regulated in colorectal [Notterman *et al*., 2001], lung [Isler *et al*.,2004] and prostate cancers [Claeskens *et al*., 2000; Nelson *et al*., 1998]. Other work has shown up regulation of SPARCL1 in cancer cells including renal cell carcinoma [Gerritsen *et al*., 2002], pancreatic adenocarcinoma [Sasaki *et al*., 2004], and on the luminal duct epithelial cells of human endometrial adenocarcinoma [Brekken *et al*., 2004]. Berekken and coworkers [2004] suggested that these differences might be resolved by time-course studies of tumor development and evaluating the type and degree of adhesion.

In the reverse comparison when PND 28 was the tester and PND 0 the driver, gene products that had greater expression at Day 28 versus Day 0 were identified. Two different types of collagen were identified, pro alpha 2 (I) collagen (COL1A2) and type III procollagen (COL3A1), transcripts with strong similarity to human 40S ribosomal protein S6, and Polymerase (RNA) II (DNA directed) polypeptide (POLR2B / RPB2). Procollagen types I-III are fibrilar and the propeptide segments must be extracellularly cleaved before the mature proteins can undergo fiber formation [Bornstein, 1980]. Type III often colocalizes with type I at a 1:5 ratio in the rat uterus [Hurst *et al.*, 1994]. Type I collagen is the most common structural collagen in the human uterus [Hurst *et al.*, 1994]

throughout the myometrium. In the rat, is has been suggested that progesterone regulates adult uterine tissue remodeling [Shynlova *et al.*, 2004] as evident after the administration of exogenous progesterone inhibited collagenase expression [Koob and Jeffrey, 1974] and increased total amount of collagen. Expression of these two procollagens in the neonatal pig uterus is likely to be determined by the early expression of SPARCL1 and presence of growth factors.

Identification of a clone with similarity to human 40S may indicate a gene that contributes to the control of cell growth and proliferation. Human 40S controls cell growth and proliferation through the selective translation of particular classes of mRNA [O'Connor *et al.*, 2003]. Increased expression of this factor at PND 0 when compared to PND 28 makes since being that at birth, the neonate uterus is actively initiating increased cellular activity including the proliferation and migration of GE from the LE at PND 0.

A second RNA Polymerase II subunit was identified in the reverse subtraction. In this comparison, POLR2B was isolated. It is otherwise known as RBP2 and is the second largest RNA binding protein of the Polymerase II subassembly. Similar to POLR2C, POLR2B acts as a scaffolding protein to recruit additional translation factors for mRNA translation [Kozlov *et al*, 2001].

The PND 28 versus PND 56 comparison resulted in fewer differentially expressed genes and only one novel gene was detected. This is not too surprising since morphologically there is a continuation of branching morphogenesis, instead of dramatic remodeling events that are associated with the initiation of gland budding and proliferation. Therefore, qRT-PCR was not performed for either forward or reverse subtraction.

Quantitative RT-PCR of SPARCL1 and clone PND 28 vs. PND 0 #7 both showed a significant increase during the proliferative stage of uterine development.

Clone PND 28 vs. PND 0 #7 did not show a difference in expression between PND 0 and 28, as anticipated. A contrast between differential screening analysis and qRT-PCR results is possible due to objective interpretation of spot intensity on each DIG-labeled membrane. Although the two PNDs in comparison were different for clone PND 28 vs. PND 0 #7, the qRT-PCR results helped further identify the time period that may be crucial to successful postnatal uterine development in the pig. Clone PND 0 vs. PND 28 #47 did not show significant difference in fold expression at any PND evaluated, but did indicate a trend for greater expression at PND 14, similar to SPARCL1 and clone PND 28 vs. PND 0 #7.

Little is known about the function of SPARCL1 in the neonatal porcine uterus other than it has high expression at PND 0 and 14 when compared to PND 28, 42, and 56. High expression of SPARCL1 at PND 0 and 14 is at the same time when uterine glands are undergoing morphological changes and cells are proliferating and migrating during budding and tubulogenesis. These events suggest an association with GE migration through the uterine stroma. This study adds further support to the contention that anti-adhesive molecules may contribute to the morphogenesis of the neonatal pig uterus.

Interpretation for the qRT-PCR profiles of the other two clones is difficult since there is no known function as of yet. Further analysis such as tissue localization for the specific products should aid in better identification for the function of these gene expression profiles in the neonatal pig uterus.

Overall, results of SSH showed that the period of postnatal growth from Day 0 to 28 has much more different activity than from Day 28 to 56. These data agree with the morphological events that occur during postnatal growth of the pig uterus. From day 0 to 28, glands emerge from simple depressions at the LE, penetrate the underlying stroma to form tubes, then actively undergo lateral side branching. After PND 28, there is no

initiation of new morphological events as branching morphogenesis continues through PND 56.

In summary, the current work identified a time period critical for the establishment and successful development of neonatal porcine uterine glands. Expression levels for all three transcripts evaluated showed a similar pattern of high levels at PND 0 and 14, then declining to normalized values at PND 28, 42, and 56. Therefore, we conclude that the factors responsible for the initiation of uterine glands are activated at birth, when only buds are present, through PND 14, when glands are forming tubes. These high levels of different transcripts may serve to regulate glandular epithelium migration through the stroma during glandular budding and tubulogenesis. Meanwhile, increased expression of transcripts are most likely establishing an appropriate microenvironement for the initiation of branching morphogenesis at PND 28. Clearly, further analysis of SPARCL1 in the pig is necessary to determine if this molecule can interact with other ECM molecules to promote and enhance uterine gland development. Identifying mRNA expression in late fetal development through early postnatal development would help determine the onset and expression profile of SPARCL1 in the pig uterus. Additional studies such as *in situ* hybridization and protein expression would further aid in clarification of the role SPARCL1 in the neonatal pig uterus. Furthermore, it would be interesting to examine the expression of growth factors and collagen in the uterus following the treatment of neonate gilts over a timecourse with exogenous SPARCL1 to see whether uterine gland development is enhanced. If this is true, it would be possible to increase uterine capacity and the number of uterine glands, so that GE can secrete greater amounts of histotroph into the uterine lumen to promote early conceptus survival.

Literature Cited

Altschul SF, Gish W, Miller W, Meyers EW and Lipman DJ. Basic local alignment search tool. J Mol Bio 1990; 215: 403-410.

Atkinson BA, King GJ and Amoroso EC. Development of the caruncular and intercaruncular regions in the bovine endometrium. Biol Reprod 1984; 30: 763-774.

Baker J, Hardy MP, Zhou J, Bondy C, Lupu F, Bellve AR and Efstratiadis A. Effects of an Igf1gene null mutation on mouse reproduction. Mol Endo 1996; 10: 903-918.

Bal HS and Getty R. Postnatal growth of the swine uterus from birth to six months. Growth 1970; 34: 15-30.

Bartol FF, Wiley AA and Goodlett DR. Ovine uterine morphogenesis: Histochemical aspects of endometrial development in the fetus and neonate. J An Sci 1988a; 66: 1303-1313.

Bartol FF, Wiley AA, Coleman DA, Wolfe DF and Riddell MG. Ovine uterine morphogenesis: Effects of age and progestin administration and withdrawal on neonatal endometrial development and DNA synthesis. J An Sci 1988b; 66: 3000-3009.

Bartol FF, Wiley AA, Spencer TE, Vallet JL and Christenson RK. Early uterine development in pigs. In: Foxcroft GR, Hunter MG and Doberska C (eds.), Control of Pig Reproduction IV, vol. 48. Essex, UK: Journal of Reproduction and Fertility Supplement; 1993: 99-116.

Bazer FW. Uterine protein secretions: Relationship to development of the conceptus. J An Sci 1975; 41: 1376-1382.

Bazer FW and Roberts RM. Biochemical aspects of conceptus-endometrial interactions. J Exper Zool 1983; 228: 373-383.

Bazer FW, Marengo SR, Geisert RD and Thatcher WW. Exocrine versus endocrine secretion of prostaglandin F2α in the control of pregnancy in swine. Anim Repr Sci 1984; 7: 115-132.

Bazer FW, Spencer TE and Ott TL. Interferon tau: a novel pregnancy recognition signal. Am J Reprod Imm 1997; 37: 412-420.

Beer H-D, Florence C, Dammeier J, McGuire L, Werner S and Duan DR. Mouse fibroblast growth factor 10: cDNA cloning, protein characterization, and regulation of mRNA expression. Oncogene 1997; 15: 2211-2218.

Beier HM. The discovery of uteroglobin and its significance for reproductive biology and endocrinology. Ann NY Ac Sci 2000; 923: 9-24.

Bell SC. Secretory endometrial/decidual proteins and their functions in early pregnancy. In: Templeton A and Weir BJ (eds.), The early days of pregnancy, vol. 36. Dorchester: Journal of Reproduction and Fertility; 1988: 109-125.

Bellusci S, Gringley J, Emoto H, Itoh N and Hogan BLM. Fibroblast growth factor 10 (FGF10) and branching morphogenesis in the embryonic mouse lung. Dev 1997; 124: 4864-4878.

Bernfield MR. Organization and remodeling of the extracellular matrix in morphogenesis. In: Connelly TG (ed.), Morphogenesis and pattern formation. New York: Raven Press; 1981: 139-162.

Bornstein P. Structurally distinct collagen types. Ann Rev Bioch 1980; 49: 957-1003.

Bottaro DP, Rubin JS, Faletto DL, Chan AM-L, Kmiecik TE, Vande Woude GF and Aaronson SA. Identification of the hepatocyte growth factor receptor as the *c-met* proto-oncogene product. Science 1991; 251: 4995.

Bradshaw AD and Sage HE. SPARC, a matricellular protein that functions in cellular differentiation and tissue response to injury. J Clin Invest 2001; 107: 1049-1054.

Branham WS, Sheehan DM, Zehr DR, Medlock KL, Nelson CJ and Ridlon E. Inhibitiion of rat uterine gland genesis by tamoxifen. Endocrin 1985; 117: 2238-2248.

Brekken RA, Sullivan MM, Workman G, Bradshaw AD, Carbon J, Siadak A, Murri C, Framson PE and Sage EH. Expression and characterization of murine hevin (SC1), a member of the SPARC family of matricellular proteins. J Histochem Cytochem 2004; 52(6): 735-48.

Buhi W, Bazer FW, Ducsay CD, Chun PW and Roberts RM. Iron content, molecular weight and possible function of progesterone-induced purple glycoprotein of the porcine uterus. Fed Proc 1979; 38: 733.

Cerro JA and Pintar JE. Insulin-like growth factor binding protein gene expression in the pregnant rat uterus. Dev Bio 1997; 18: 278-295.

Chen C, Spencer TE and Bazer FW. Fibroblast growth factor-10: a stromal mediator of epithelial function in the ovine uterus. Biol Reprod 2000; 63: 959-966.

Claeskens A, Ongenae N, Neefs JM, Cheyns P, Kaijen P, Cools M, Kutoh E. Hevin is down-regulated in many cancers and is a negative regulator of cell growth and proliferation. Br J Cancer 2000; 82(6): 1123-30.

Clawitter J, Trout WE, Burke MG, Araghi S and Roberts RM. A novel family of progesterone-induced, retinol-binding proteins from uterine secretions of the pig. J Biol Chem 1990; 265: 3248-3255.

Cooke PS, Buchanan DL, Lubahn DB and Cunha GR. Mechanism of Estrogen Action: Lessons from the Estrogen Receptor- Knockout Mouse. Biol Reprod 1998; 59: 470-475.

Corner GW. Cyclic changes in the ovaries and uterus of the sow, and their relation to the mechanism of implantation. Contr Embry 1921; 64: 117-146.

Couse JF, Curtis SW, Washburn TF, Lindzey J, Golding TS, Lubahn DB, Smithies O and Korach KS. Analysis of transcription and estrogen insensitivity in the female mouse after targeted disruption of the estrogen receptor gene. Mol Endocrinol 1995; 9: 1441-1454.

Cunha GR. Stromal induction and specification of morphogenesis and cytodifferentiation of the epithelia of the mullerian ducts and urogenital sinus during development of the uterus and vagina in mice. J Exp Zool 1976; 196: 361-370.

Cunha GR and Lung B. The importance of stroma in morphogenesis and functional activity of urogenetal epithelium. In Vitro 1979; 15: 50-71.

Cunha GR, Chung LWK, Shannon JM, Taguchi O and Fujii H. Hormone induced morphogenesis and growth: role of mesenchymal-epithelial interactions. Recent Prog Horm Res 1983; 39: 559-595.

DeSouza MM, Surveyor GA, Price RE, Julian J, Kardon R, Zhou X, Gendler S, Hilkens J and Carson DD. Muc1/episialin: a critical barrier in the female reproductive tract. J Reprod Imm 2000; 45: 127-158.

Dhindsa DS, Dziuk PJ, Norton HW. Time of transuterine migration and distribution of embryos in the pig. Anat Rec 1967; 159(3): 325-330.

Diatchenko L, Lau Y-FC, Campbell AP, Chenchik A, Moqadam F, Huang B, Lukyanov S, Lukyanov K, Gurskaya N, Sverdlov ED and Siebert PD. Suppression subtractive hybridization: A method for generating differentially regulated or tissue-specific cDNA probes and libraries. PNAS 1996; 93: 6025-6030.

Dillon C, Spencer-Dane B and Dickson C. A crucial role for fibroblast growth factor signaling in embryonic mammary gland development. J Mamm Gland Bio Neo 2004; 9: 207-215.

Dunlap KA and Stormshak F. Nongenomic inhibition of oxytocin binding by progesterone in the ovine uterus. Biol Reprod 2004; 70: 65-69.

Dziadek M, Paulsson M, Aumailley M, Timpl R. Purification and tissue distribution of a small protein (BM-40) extracted from a basement membrane tumor. Eur J Biochem 1986; 161(2): 455-64.

Engel J, Taylor J, Paulsson M, Sage HE and Hogan B. Calcium binding domains and calcium-induced conformational transition of SPARC/BM-40/osteonectin, an extracellular glycoprotein expressed in mineralized and nonmineralized tissues. Biochem 1987; 26: 6958-6965.

Fazleabas AT, Bazer FW and Roberts RM. Purification and properties of a progesterone-induced plasmin/trypsin inhibitor from uterine secretions of pigs and its immunocytochemical localization in the pregnant uterus. J Biol Chem 1982; 257(12): 6886-6897.

Francki A, Bradshaw AD, Bussak JA, Howe CC, Couser WG and Sage HE. SPARC regulates the expression of collagen type I and transforming growth factor-□1 in mesangial cells. J Biol Chem 1999; 274: 32145-32152.

Geisert RD, Renegar RH, Thatcher WW, Roberts RM and Bazer FW. Establishment of pregnancy in the pig: I. Interrelationships between preimplantation development of the pig blastocyst and uterine endometrial secretions. Biol Reprod 1982a; 27: 925-939.

Geisert RD, Brooban, JW, Roberts RM and Bazer FW. Establishment of pregnancy in the pig: II. Cellular remodeling of the porcine blastocyst during elongation on day 12 of pregnancy. Biol Reprod 1982b; 27: 941-955.

Geisert RD, Thatcher WW, Roberts RM and Bazer FM. Establishment of pregnancy in the pig: III. Endometrial secretory response to estradiol valerate administered on day 11 of the estrous cycle. Biol Reprod 1982c; 27: 957-965.

Geisert RD, Zavy MT, Wettemann RP and Biggers BG. Length of pseudopregnancy and pattern of uterine protein release as influenced by time and duration of oestrogen administration in the pig. J Reprod Fertil 1987; 79(1): 163-72.

Geisert RD, Zavy MT, Moffatt RJ, Blair RM and Yellin T. Embryonic steroids and the establishment of pregnancy in pigs. In: Cole DJA, Foxcroft GR and Weir BJ (eds.), Control of pig reproduction III, vol. 40. Dorchester: Journal of Reproduction and Fertility; 1990: 293-305.

Geisert RD, Brenner RM, Moffatt RJ, Harney JP, Yellin T and Bazer FW. Changes in oestrogen receptor protein, mRNA expression and localization in the endometrium of cyclic and pregnant gilts. Repr Fert Dev 1993; 5: 247-260.

Geisert RD, Pratt TN, Bazer FW, Mayes JS and Watson GH. Immunocytochemical localization and changes in endometrial progestin receptor protein during the porcine oestrous cycle and early pregnancy. Repr Fert Dev 1994; 6: 749-760.

Girard J-P and Springer TA. Modulation of endothelial cell adhesion by hevin, an acidic protein associated with high endothelial venules. J Biol Chem 1996; 271(8): 4511-4517.

Gerritsen ME, Peale FV Jr and Wu T. Gene expression profiling in silico: relative expression of candidate angiogenesis associated genes in renal cell carcinomas. Exp Nephrol 2002; 10(2): 114-9.

Grange T, Martins de Sa C, Oddos J and Pictet R. Human mRNA polyadenylate binding protein: evolutionary conservation of a nucleic acid binding motif. Nucl Acids Res 1987; 15: 4771-4787.

Gray CA, Bartol FF, Taylor KM, Wiley AA, Ramsey WS, Ott TL, Bazer FW and Spencer TE. Ovine uterine gland knock-out model: Effects of gland ablation on the estrous cycle. Biol Reprod 2000a; 62: 448-456.

Gray CA, Taylor KM, Bazer FW and Spencer TE. Mechanisms regulating norgestomet inhibition of endometrial gland morphogenesis in the neonatal ovine uterus. Mol Reprod Dev 2000b; 57: 67-78.

Gray CA, Bazer FW and Spencer TE. Effects of neonatal progestin exposure on female reproductive tract structure and function in the adult ewe. Biol Reprod 2001a; 64: 797-804.

Gray CA, Bartol FF, Tarleton BJ, Wiley AA, Johnson GA, Bazer FW and Spencer TE. Developmental biology of uterine glands. Biol Reprod 2001b; 65: 1311-1323.

Gray CA, Taylor KM, Ramsey WS, Hill JR, Bazer FW, Bartol FF and Spencer TE. Endometrial glands are required for preimplantation conceptus elongation and survival. Biol Reprod 2001c; 64: 1608-1613.

Gray CA, Burghardt RC, Johnson GA, Bazer FW and Spencer TE. Evidence that absence of endometrial gland secretions in uterine gland knockout ewes compromises conceptus survival and elongation. Reproduction 2002; 124: 289-300.

Gries LK, Geisert RD, Zavy MT, Garrett JE and Morgan GL. Uterine secretory alterations coincident with embryonic mortality in the gilt after exogenous estrogen administration. J An Sci 1988; 67: 276-284.

Hadek R and Getty R. The changing morphology in the uterus of the growing pig. Am J Vet Res 1959: 573-577.

Hammond JM, Samaras S, Grimes R, Leighton J, Barber JA, Canning SF and Guthrie H. The role of insulin-like growth factors and epidermal growth factor-related peptides in intraovarian regulation in the pig ovary. In: Foxcroft GR, Hunter MG and Doberska C (eds.), Control of Pig Reproduction IV, vol. 48. Dorchester: Journal of Reproduction and Fertility; 1993: 117-125.

Hansen PJ, Bazer FW and Roberts RM. Appearance of beta-hexosaminidase and other lysosomal-like enzymes in the uterine lumen of gilts, ewes and mares in response to progesterone and oestrogens. J Reprod Fertil 1985; 73(2): 411-424.

Hurst PR, Gibbs RD, Clark DE and Myers DB. Temporal changes to uterine collagen types I, III and V in relation to early pregnancy in the rat. Repr Fert Dev 1994; 6: 669-677.

Igarashi M, Finch PW and Aaronson SA. Characterization of recombinant human fibroblast growth factor (FGF)-10 reveals functional similarities with keratinocyte growth factor (FGF-7). J Biol Chem 1998; 273: 13220-13235.

Isler SG, Schenk S, Bendik I, Schraml P, Novotna H, Moch H, Sauter G and Ludwig CU. Genomic organization and chromosomal mapping of SPARC-like 1, a gene downregulated in cancers. Int J Oncol 2001; 18: 521-526.

Isler SG, Ludwig CU, Chiquet-Ehrismann R and Schenk S. Evidence for transcriptional repression of SPARC-like 1, a gene downregulated in human lung tumors. Int J Oncology 2004; 25: 1073-1079.

Johnson GA, Spencer TE, Burghardt RC and Bazer FW. Ovine osteopontin: I. Cloning and expression of messenger ribonucleic acid in the uterus during the periimplantation period. Biol Reprod 1999a; 61: 884-891.

Johnson GA, Burghardt RC, Spencer TE, Newton GR, Ott TL and Bazer FW. Ovine osteopontin: II. Osteopontin and αvβ3 integrin expression in the uterus and conceptus during the periimplantation period. Biol Reprod 1999b; 61: 892-899.

Johnson GA, Bazer FW, Jaeger LA, Ka H, Garlow JG, Prarrer C, Spencer TE and Burghardt RC. Muc-1, integrin, and osteopontin expression during the implantion cascade in sheep. Biol Reprod 2001; 65: 820-828.

Johnston IG, Paladino T, Gurd JW and Brown IR. Molecular cloning of SC1: a putative extracellular matrix glycoprotein showing partial similarity to osteonectin/BM40/SPARC. Neuron 1990; 2: 165-176.

Katzenellenbogen BS. Estrogen receptors: bioactivities and interactions with cell signaling pathways. Biol Reprod 1996; 54: 287-293.

Kennedy JP, Worthington CA and Cole ER. The post-natal development of the ovary and uterus of the Merino lamb. J Reprod Fert 1974; 36: 275-282.

King GJ, Atkinson B A and Robertson HA. Development of the bovine placentome from days 20 to 29 of gestation. J Reprod Fert 1980; 59: 95-100.

King GJ, Atkinson B A and Robertson HA. Development of the intercaruncular areas during early gestation and establishment of the bovine placenta. J Reprod Fert 1981; 61: 469-474.

Kleinberg DL. IGF-I: An essential factor in terminal end bud formation and ductal morphogenesis. J Mammary Gland Biol Neopl 2000; 5: 7-17.

Knight JW, Bazer FW and Wallace HD. Effects of superovulation and unilateral ovariectomy-hysterectomy on porcine uterine protein secretions. J Anim Sci 1973; 36(1): 61-65.

Komatsu M, Carothers Carraway CA, Fregien NL and Carraway KL. Reversible disruption of cell-matrix and cell-cell interactions by overexpression of sialomucin complex. J Biol Chem 1997; 272: 33245-33254.

Koob TJ and Jeffrey JJ. Hormonal regulation of collagen degradation in the uterus: inhibition of collagenase expression by progesterone and cyclic AMP. Biochim Biophys Acta 1974; 354: 61–70.

Korach KS. Insights from the study of animals lacking functional estrogen receptor. Science 1994; 266: 1524-1527.

Kozlov G, Trempe J-F, Khaleghpour K, Kahwejian A, Ekiel I and Gehring K. Structure and function of the C-terminal PABC domain of humal poly(A)-binding protein. PNAS 2001; 98: 4409-4413.

Lane TF and Sage EH. The biology of SPARC a protein that modulates cell-matrix interactions. FASEB J 1994; 8: 163-173.

Lee JM. The role of protein elongation factor EF1A2 in ovarian cancer. Reprod Bio Endo 2003; 1: 69.

Lu W, Luo Y, Kan M and McKeehan WL. Fibroblast growth factor-10: a second candidate stromal to epithelial cell andromedin in prostate. J Biol Chem 1999; 274: 12827-12834.

Lubahn DB, Moyer JS, Golding TS, Couse JF, Korach KS and Smithies O. Alteration of reproductive function but not prenatal sexual development after insertional disruption of the mouse estrogen receptor gene. PNAS 1993; 90: 11162-11166.

Marion GB and Gier HT. Ovarian and uterine embryogenesis and morphology of the non-pregnant female mammal. J An Sci Supp 1971; 32: 24-47.

Mason IJ, Murphy D, Munke M, Francke U, Elliott RW and Hogan BL. Developmental and transformation-sensitive expression of the SPARC gene on mouse chromosome 11. EMBO J. 1986; 5(8): 1831-1837.

Maurer P, Hohenadl C, Hohenester E, Gohring W, Timpl R and Engel J. The C-terminal portion of BM-40 (SPARC/Osteonectin) is an autonomously folding and crystallisable domain that binds calcium and collagen IV. J Mol Biol 1995; 253: 347-357.

Maurer P, Gohring W, Sasaki T, Mann K, Timpl R and Nischt R. Recombinant and tissue-derived mouse BM-40 bind to several collagen types and have increased affinities after proteolytic activation. Cell Mol Life Sci 1997; 53: 478-484.

Morgan GL, Geisert RD, Zavy MT and Fazleabas AT. Development and survival of pig blastocysts after oestrogen administration on day 9 or days 9 and 10 of pregnancy. J Reprod Fertil 1987 May; 80(1): 133-141.

Mossmann HW. Vertebrate fetal membranes: comparative ontogeny and morphology, evolution, phylogenetic significance, basic functions, research opportunities. New Brunswick: Rutgers University Press; 1987: 63-73.

Mossman HW. Comparative Anatomy. In: Wynn RM and Jollie WP (eds.), Biology of the Uterus. New York: Plenum; 1989: 19-34.

Murphy LJ and Ghahary A. Uterine insulin-like growth factor-1: regulation of expression and its role in estrogen-induced uterine proliferation. Endocr Rev 1990; 11: 443-453.

Nelson PS, Plymate SR, Wang K, True LD, Ware JL, Gan L, Liu AY and Hood L. Hevin, an antiadhesive extracellular matrix protein, is down-regulated in metastatic prostate adenocarcinoma. Cancer Res 1998; 58(2): 232-236.

Nomura S, Wills AJ, Edwards DR, Heath JK and Hogan BLM. Developmental expression of 2ar (osteopontin) and SPARC (osteonectin) RNA as revealed by in situ hybridization. J Cell Bio 1988; 106: 441-450.

Norbert Schuster N and Krieglstein K. Mechanisms of TGF-β-mediated apoptosis. Cell Tiss Res, 2002; 307(1): 1-14.

Notterman DA, Alon U, Sierk AJ and Levine AJ. Transcriptional gene expression profiles of colorectal adenoma, adenocarcinoma, and normal tissue examined by oligonucleotide arrays. Cancer Res 2001; 61(7): 3124-3130.

O'Connor PMJ, Kimball SR, Suryawan A, Bush JA, Nguyen HV, Jefferson LS and Davis TA. Regulation of translation initiation by insulin and amino acids in skeletal muscle of neonatal pigs. Am J Physiol Endocrinol Metab 2003; 285(1): E40-53.

Ott TL, Yin J, Wiley AA, Kim H-T, Behzad G-N, Spencer TE, Bartol FF, Burghardt RC and Bazer FW. Effects of the estrous cycle and early pregnancy on uterine expression of Mx protein in sheep (*Ovis aries*). Biol Reprod 1998; 59: 784-794.

Park WY, Miranda B, Lebeche D, Hashimoto G and Cardoso WV. FGF-10 is a chemotactic factor for distal epithelial buds during lung development. Dev Bio 1998; 201: 125-134.

Perry JS and Rowlands IW. Early pregnancy in the pig. J Reprod Fert 1962; 4: 175-188.

Pollard JW. Tumour-stromal interactions: Transforming growth factor-beta isoforms and hepatocyte growth factor/scatter factor in mammary gland ductal morphogenesis. Breast Canc Res 2001; 3: 230-237.

Powers CJ, McLeskey SW and Wellstein A. Fibroblast growth factors, their receptors and signaling. Endoc Rel Canc 2000; 7(3): 165-197.

Reilas T and Katila T. Proteins and enzymes in uterine lavage flud of postpartum and nonparturient mares. Reprod Domest Anim 2002; 37: 261-268.

Roberts RM, Bazer FW, Baldwin N and Pollard WE. Progesterone induction of lysozyme and peptidase activities in the porcine uterus. Arch Biochem Biophys 1976; 177(2): 499-507.

Roberts RM and Bazer FW. The functions of uterine secretions. J Reprod Fert 1988; 82: 875-892.

Roberts RM, Xie S and Trout W. Embryo-uterine interactions in pigs during week 2 of pregnancy. In: Foxcroft GR, Hunter MG and Doberska C (eds.), Control of Pig Reproduction IV. Dorchester: Journal of Reproduction and Fertility; 1993: 171-186.

Rosenzweig SA. What's new in the IGF-binding proteins? Growth Horm IGF Res 2004; 14(5): 329-336.

Rubin JS, Chan AM-L, Bottaro DP, Burgess WH, Taylor WG, Cech AC, Hirschfield DW, Wong J, Miki T, Finch PW and Aaronson SA. A broad-spectrum human lung fibroblast-derived mitogen is a variant of hepatocyte growth factor. PNAS 1991; 88: 415-419.

Sage H, Vernon RB, Funk SE, Everitt EA and Angello J. SPARC, a secreted protein associated with cellular proliferation, inhibits cell spreading in vitro and exhibits

Ca+2-dependent binding to the extracellular matrix. J Cell Biol. 1989; 109(1): 341-56.

Sage HE and Bornstein P. Extracellular proteins that modulate cell-matrix interactions. J Biol Chem 1991; 266: 14831-14834.

Sasaki T, Hohenester E, Gohring W and Timpl R. Crystal strucutre and mapping by site-directed mutagenesis of the collagen-binding epitope of an activated form of BM-40/SPARC/osteonectin. The EMBO Journal 1998; 17: 1625-1634.

Sasaki A, Ishio T, Bandoh T, Shibata K, Matsumoto T, Aramaki M, Kawano K, Kitano S, Kashima K and Yokoyama S. Clear cell carcinoma of the pancreas: an adenocarinoma with unusual phenotype of duct cell origin. J Hepatobiliary Pancreat Surg 2004; 11(2): 140-144.

Schraml P, Shipman R, Colombi M and Ludwig CU. Identification of genes differentially expressed in normal lung and non-small cell lung carcinoma tissue. Cancer Res, 1994; 54(19): 5236-5240.

Schwartz H and Darnell JE. The association of protein with the polyadenylic acid of HeLa cell messeger RNA: evidence for a "transport" role of a 75,000 molecular weight polypeptide. J Mol Bio 1976; 104: 833-851.

Sharpe PM and Ferguson MWJ. Mesenchymal influences on epithelial differentiation in developing systems. J Cell Sci Suppl 1988; 10: 195-230.

Shynlova O, Mitchell JA, Tsampalieros A, Langille BL and Lye SJ. Progesterone and gravidity differentially regulate expression of extracellular matrix components in the pregnant rat uterus. Biol Reprod 2004; 70: 986-992.

Silverman GA, Bird PI, Carrell RW, Church FC, Coughlin PB, Gettins PGW, Irving JA, Lomas DA, Luke CJ, Moyer RW, Pemberton PA, Remold-O'Donnell E, Salvesen GS, Travis J and Whisstock JC. The serpins are an expanding superfamily of structurally similar but functionally diverse proteins. Evolution, mechanism of inhibition, novel functions, and a revised nomenclature. J Biol Chem 2001; 276: 33293-33296.

Simmen RCM and Simmen FA. Regulation of uterine and conceptus secretory activity in the pig. In: Cole DJA, Foxcroft GR and Weir BJ (eds.), Control of Pig Reproduction III, vol. 40. Dorchester: Journal of Reproduction and Fertility; 1990: 279-292.

Sinowatz F and Friese AE. Uterine glads of the pig during pregnancy. An ultrastructural and cytochemical study. Anat Embryol 1983; 166: 121-134.

Soderling JA, Reed MJ, Corsa A and Sage HE. Cloning and expression of murine SC1, a gene product homologous to SPARC. J Histo Cyto 1997; 45(6): 823-835.

Song CZ, Hanada K-i, Yano K-i, Maeda Y, Yamamoto K and Muramatsu M. High conservation of subunit composition of RNA polymerase I (A) between yeast and mouse and the molecular cloning of mouse RNA polymerase I 40-kDa subunit PRA40. J Biol Chem 1994; 269: 26976-26981.

Spencer TE, Bartol FF, Wiley AA, Coleman DA and Wolfe DF. Neonatal porcine endometrial development involves coordinated changes in DNA synthesis, glycosaminoglycan distribution, and 3H-glucosamine labeling. Biol Reprod 1993a; 48: 729-740.

Spencer TE, Wiley AA and Bartol FF. Neonatal age and period of estrogen exposure affect porcine uterine growth, morphogenesis, and protein synthesis. Biol Reprod 1993b; 48: 741-751.

Spencer TE, Stagg AG, Joyce MM, Jenster G, Wood CG, Bazer FW, Wiley AA and Bartol FF. Discovery and characterization of endometrial epithelial messenger ribonucleic acids using the ovine uterine gland knockout model. Endocrin 1999; 140: 4070-4080.

Talapatra S, Wagner JDO and Thompson CB. Elongation factor-1 alpha is a selective regulator of growth factor withdrawal and ER stress-induced apoptosis. Cell Death Diff 2002; 9: 856-861.

Tarleton BJ, Wiley AA, Spencer TE, Moss AG and Bartol FF. Ovary-independent estrogen receptor expression in neonatal porcine endometrium. Biol Reprod 1998; 58: 1009-1019.

Tarleton BJ, Wiley AA and Bartol FF. Endometrial development and adenogenesis in the neonatal pig: effects of estradiol valerate and the antiestrogen ICI 182,780. Biol Reprod 1999; 61: 253-263.

Tarleton BJ, Wiley AA and Bartol FF. Neonatal estradiol exposure alters uterine morphology and endometrial transcriptional activity in prepubertal gilts. Dom Anim Endo 2001; 21: 111-125.

Tarleton BJ, Braden TD, Wiley AA and Bartol FF. Estrogen-induced disruption of neonatal porcine uterine development alters adult uterine function. Biol Reprod 2003; 68: 1387-1393.

Taylor KM, Chen C, Gray CA, Bazer FW and Spencer TE. Expression of messenger ribonucleic acids for fibroblast growth factors 7 and 10, hepatocyte growth factor, and insulin-like growth factors and their receptors in the neonatal ovine uterus. Biol Reprod 2001; 64: 1236-1246.

Termine JD, Kleinman HK, Whitson SW, Conn KM, McGarvey ML and Martin GR. Osteonectin, a bone-specific protein linking mineral to collagen. Cell 1981; 26: 99-105.

Trout WE, Hall JA, Stallings-Mann ML, Galvin JM, Anthony RV and Roberts M. Steroid regulation of the synthesis and secretion of retinol-binding protein by the uterus of the pig. Endocrin 1992; 130: 2557-2564.

Wang HS and Chard T. IGFs and IGF-binding proteins in the regulation of human ovarian and endometrial function. J Endocr 1999; 161: 1-13.

Wiley AA, Bartol FF and Barron DH. Histogenesis of the ovine uterus. J An Sci 1986; 64: 1262-1269.

Wiseman B and Werb Z. Stromal effects on mammary gland development and breast cancer. Science 2002; 296: 1046-1049.

Wu MC and Dziuk PJ. Ovarian influence on uterine growth in prepubertal gilts. J An Sci 1988; 66: 2893-2898.

Yamasaki M, Miyake A, Tagashira S and Itoh N. Structure and expression of the rat mRNA encoding a novel member of the fibroblast growth factor family. J Biol Chem 1996; 271: 15918-15921.

Yuen ST, Wong MP, Chung LP, Chan SY, Cheung N, Ho J and Leung SY. Upregulation of lysozyme production in adenomas and adenocarcinomas. Histopath 1998; 32: 126-132.

Zavy MT, Bazer FW, Thatcher WW and Wilcox CJ. A study of prostaglandin F2 alpha as the luteolysin in swine: V. Comparison of prostaglandin F, progestins, estrone and estradiol in uterine flushings from pregnant and nonpregnant gilts. Prostaglandins. 1980; 20(5): 837-851.

VITA

LEANNE MICHELLE WIER

Candidate for the Degree of

Master of Science

Thesis: EVALUATION OF GENE EXPRESSION DURING DEVELOPMENT OF THE NEONATAL PORCINE UTERUS USING SUPPRESSION SUBTRACTIVE HYBRIDIZATION

Major Field: Reproductive Physiology

Biographical:

Personal Information:

Born August 29, 1977 in San Antonio, Texas, the daughter of Glen and Diane Wier of Elgin, Texas.

Education:

Graduated from Elgin High School, Elgin, Texas in May 1995. Received Bachelor of Science from Texas A&M University - College Station in August 2000. Completed the requirements for the Master of Science degree with a major in Reproductive Physiology at Oklahoma State University in December 2004.

Experience:

Laboratory Technician, Ultimate Genetics, Franklin, TX, March 2000 to April 2001. Laboratory Technician, Oklahoma State University — Stillwater, Department of Physiological Sciences, June 2001 to January 2005.

Professional Organizations:

Society for the Study of Reproduction, Phi Kappa Phi Scientific Research Society, Oklahoma Microscopy Society.

Name: Leanne Wier Date of Degree: December 2004

Institution: Oklahoma State University Location: Stillwater, Oklahoma

Title of Study: EVALUATION OF GENE EXPRESSION DURING DEVELOPMENT OF THE NEONATAL PORCINE UTERUS USING SUPPRESSION SUBTRACTIVE HYBRIDIZATION.

Pages in Study: 92 Candidate for the Degree of Master of Science

Major Field: Animal Science

Scope and Method of Study: Specific changes in gene expression involved in the completion of uterine gland development during the first 56 days of postnatal growth in the pig have not been well described or understood. The present work utilized suppression subtractive hybridization (SSH) to create unique cDNA libraries respective to postnatal development at 3 stages: Day 0 when only shallow depressions can be observed, Day 28 when branching morphogenesis begins, and Day 56 when glands are well established.

Findings and Conclusions: A total of 288 SSH products were screened in two forward and reverse reactions. Of these, 67 were identified to be differentially expressed through dot-blot hybridization assays using DIG-labeled probes. Only 34 were subjected to sequencing and BLAST analysis. Sequence analysis revealed 25/34 quality readings and 16/25 matched known sequences, while 7/25 returned identity to uncharacterized clones, and 2/25 had no significant match to any known sequences. Comparison of PND 0 with PND 28 showed genes in the forward subtraction represent those involved in transcription or translation, including elongation factor 1 alpha 1 (EF1a1), poly(A) binding protein, cytoplasmic 1 (PABPC1), and polymerase (RNA) II (DNA directed) polypeptide C (POLR2C / RPB3). One other gene of interest found was secreted protein, acidic, cysteine-rich-like 1 (SPARCL1) which influences several cellular activities including proliferation, migration, and differentiation. Gene products that had greater expression at Day 28 than Day 0 included type II procollagen (COL1A2) and type III procollagen (COL3A1) which are important in tissue structure. Also identified in the reverse subtraction was a clone with strong similarity to human 40S, which may indicate a gene that contributes to the control of cell growth and proliferation. The PND 28 versus PND 56 comparison resulted in fewer differentially expressed genes and only one novel gene was detected. Quantitative real-time PCR (qRT-PCT) assays were performed for SPARCL1 and two uncharacterized clones. Expression levels for all three transcripts evaluated showed a similar pattern of high levels at PND 0 and 14, then declining to normalized values at PND 28, 42, and 56. Therefore, we conclude that the factors responsible for the initiation of uterine glands are activated at birth, when only buds are present, through PND 14, when glands are forming tubes. These high levels of different transcripts may serve to regulate glandular epithelium migration through the stroma during glandular budding and tubulogenesis.

Advisor's Approval: _____